Zircon U–Pb geochronology, Lu–Hf isotope systematics, and geochemistry of bimodal volcanic rocks and associated granitoids from Kotri Belt, Central India: Implications for Neoarche…

Article *in* Gondwana Research · January 2016

DOI: 10.1016/j.gr.2015.12.008

CITATIONS
38

READS
776

10 authors, including:

Prof. Dr. C. Manikyamba
National Geophysical Research Institute
114 PUBLICATIONS **2,381** CITATIONS
SEE PROFILE

M. Santosh
China University of Geosciences (Beijing)
1,454 PUBLICATIONS **44,961** CITATIONS
SEE PROFILE

Dr. Chandan Kumar B
Central University of Kerala
35 PUBLICATIONS **112** CITATIONS
SEE PROFILE

Li Tang
China University of Geosciences (Beijing)
56 PUBLICATIONS **961** CITATIONS
SEE PROFILE

Zircon U-Pb geochronology, Lu-Hf isotope systematics, and geochemistry of bimodal volcanic rocks and associated granitoids from Kotri Belt, Central India: Implications for Neoarchean-Paleoproterozoic crustal growth

C. Manikyamba, M. Santosh, B. Chandan Kumar, S. Rambabu, Li Tang, Abhishek Saha, Arubam C. Khelen, Sohini Ganguly, Th. Dhanakumar Singh, D.V. Subba Rao

PII: S1342-937X(16)00033-2
DOI: doi: 10.1016/j.gr.2015.12.008
Reference: GR 1567

To appear in: *Gondwana Research*

Received date: 7 September 2015
Revised date: 24 November 2015
Accepted date: 6 December 2015

Please cite this article as: Manikyamba, C., Santosh, M., Kumar, B. Chandan, Rambabu, S., Tang, Li, Saha, Abhishek, Khelen, Arubam C., Ganguly, Sohini, Singh, Th. Dhanakumar, Rao, D.V. Subba, Zircon U-Pb geochronology, Lu-Hf isotope systematics, and geochemistry of bimodal volcanic rocks and associated granitoids from Kotri Belt, Central India: Implications for Neoarchean-Paleoproterozoic crustal growth, *Gondwana Research* (2016), doi: 10.1016/j.gr.2015.12.008

Zircon U-Pb geochronology, Lu-Hf isotope systematics, and geochemistry of bimodal volcanic rocks and associated granitoids from Kotri Belt, Central India: implications for Neoarchean-Paleoproterozoic crustal growth

C. Manikyamba[a], M. Santosh[b,c], B. Chandan Kumar[a,d], S. Rambabu[a], Li Tang[c], Abhishek Saha[a,e], Arubam C Khelen[a], Sohini Ganguly[a, f], Th. Dhanakumar Singh[a], D.V. Subba Rao[a]

[a]*National Geophysical Research Institute (Council of Scientific and Industrial Research), Uppal Road, Hyderabad 500 007*
[b]*Centre for Tectonics, Resources and Exploration, Department of Earth Sciences, University of Adelaide, SA 5005, Australia*
[c]*School of Earth Science and Resources, China University of Geosciences, Beijing, China*
[d]*Karnatak University, Pavatenagar, Dharwad-580007, India*
[e]*National Institute of Oceanography (Council of Scientific and Industrial Research), Regional Centre, Visakhapatnam 530017*
[f]*Department of Geology, Andhra University, Visakhapatnam 530017*

*E-mail: cmaningri@gmail.com

Abstract

The Bastar Craton of Central India has a thick sequence of volcano-sedimentary rocks preserved in Kotri-Dongargarh belt that developed on a tonalite-trondhjemite-granodiorite (TTG) basement followed upwards by the Amgaon, Bengpal, Bailadila and Nandagaon Groups of rocks. Here, we report the U-Pb geochronology and Lu-Hf isotope systematic and whole rock geochemistry of volcanic rocks and associated granitoids belonging to the Pitapani basalts, Bijli rhyolites and Dongargarh granite in the Nandagaon Group of the Kotri belt. The volcanic rocks of Nandagaon Group are bimodal in nature in which the basalts exhibit intergranular, porphyritic to spherulitic texture composed of pyroxenes, plagioclase, tremolite, actinolite, chlorite ± Fe oxides. The rhyolites display porphyritic texture consisting of K-feldspar, quartz and plagioclase as phenocrysts. The associated porphyritic granitoids have K-feldspar, microcline, plagioclase and biotite phenocrysts within a groundmass of

similar composition. The bimodal suite displays LILE, LREE enrichment and HFSE depletion with significant negative Nb-Ta anomalies combined with slightly fractionated REE patterns in the basalts and highly fractionated patterns and prominent negative Eu anomalies in the rhyolites endorsing their generation in an island arc/back arc tectonic setting. The geochemical features of the associated granitoids indicate that these are potassic and classify as within plate A-type granites. Zircons from the basalts show clear oscillatory zoning in their CL images. They cluster as a coherent group with $^{207}Pb/^{206}Pb$ spot ages ranging from 2446 to 2522 Ma and weighted mean age of 2471±7 Ma. Zircons from the rhyolite samples are subhedral to euhedral and show simple oscillatory zoning with some heterogeneous fractured domains. The data from two samples define upper intercept ages of 2479±13 Ma and 2463±14 Ma. Zircons grains in the granite show clear oscillatory zoning and their U-Pb data define an upper intercept age of 2506±50 Ma. The Lu-Hf isotopic data on the zircons from the basalts show initial $^{176}Hf/^{177}Hf$ ratios from 0.280925 to 0.281018. Their $\varepsilon_{Hf}(t)$ values are in the range of -10.0 to -6.7. The Hf depleted model ages (T_{DM}) are between 3038 Ma and 3171 Ma, and Hf crustal model ages (T_{DM}^{C}) varies from 3387-3589 Ma. The zircons from the rhyolites show initial $^{176}Hf/^{177}Hf$ ratios from 0.280919 to 0.281020 and 0.281000 to 0.281103 respectively with $\varepsilon_{Hf}(t)$ values are varying from -10 to -6.4 and -7.5 to -3.9. Among these, one sample shows T_{DM} between 3038 Ma and 3182 Ma, and T_{DM}^{C} varies from 3377-3596 Ma whereas the other sample shows ages of 2925 Ma and 3072 Ma with T_{DM}^{C} varying from 3208-3432 Ma. The initial $^{176}Hf/^{177}Hf$ ratios of the granites range from 0.280937 to 0.281062 with $\varepsilon_{Hf}(t)$ values of -8.8 to -4.3. The T_{DM} shows a range of 2979 Ma and 3170 Ma, and T_{DM}^{C} varies from 3269-3541 Ma. The predominant negative $\varepsilon_{Hf}(t)$ values of zircons from these rocks suggest that the source material was evolved from the Paleoarchean crust. The geological, geochemical and geochronological evidence suggests coeval tectonic and magmatic episodes of volcanic and plutonic activity in an island arc

setting where the arc migrated towards the continental margin and played a significant role – in the Neoarchean- Paleoproterozoic crustal growth of the Kotri belt of Central India.

Keywords: U-Pb zircon geochronology, Lu-Hf isotopes, Bimodal volcanics, Granites, Kotri belt.

1. Introduction

Synchronous mafic and felsic volcanism are reported from different tectonic settings such as intracontinental rift, back arc basin, island arc, active and passive continental margins and within plate extensional settings (Duncan et al., 1984; Garland et al., 1995; Pin and Marini, 1993; Turner et al., 1992; Frost et al., 1999; Frost and Frost, 1997; Frey et al., 1984; Pin and Paquette, 1997; Zhang et al., 2008). The bimodal association of basalt and rhyolite has been genetically correlated with mantle plume activities by several workers (Li et al., 2002, 2003, 2005; Jordan et al., 2004; Dobretsov, 2005). In some cratonic stratigraphy, coeval or younger granitoid magmatism is also documented along with the eruption of bimodal volcanic rocks. In most of the cases, basalt and rhyolite are two most important components of bimodal volcanism with distinct absence of any intermediate counterparts (Moraes et al., 2003; Li et al., 2002, 2005). The absence of intermediate volcanic rocks in the whole sequence has been described as the "Daly Gap" (Daly, 1925; Bonnefoi et al., 1995). In a rift environment, the melting of the mantle source produces melts that underplate and accumulate within the lower crust which transfer heat and fluids to the overlying crust in an extensional setting causing partial melting and generating felsic rocks of the bimodal suite. As a consequence of this, magmas derived from the mantle and the overlying crust erupt at the same time with extension, giving rise to the bimodal suite (Cox, 1988; Rudnick, 1990; Vernon, 1983; Weinverg, 1997; Barbarin, 2005; Ahmad et al., 2009). Contrary to this, in a subduction zone environment, a three component mixing model has been envisaged by some workers for the generation of arc lavas which involve mantle wedge, subducting slab and associated sediments. The LILE, LREE enrichment and HFSE depletion are considered as characteristic geochemical signatures inherited from the three component mixing process (Ellam and Hawkesworth, 1988; Hawkesworth et al., 1991; Saunders et al., 1991).

The Kotri-Dongargarh Supergroup of Bastar Craton represents supracrustal rocks consisting of greenstone-granite affinity. The basement of this Supergroup consists of migmatites, TTG and biotite granite with BIF, quartzite, metaarkose and high grade schistose rocks of the Bengpal Group (Sivakumar et al., 2012). The gneiss and supracrustal rocks are intruded by NW-SE dyke swarms. The volcanic sequence of Dongargarh Group is composed of basaltic flows with intermediate volcanic rocks and relatively low felsic flows known as Bijli rhyolites. Bimodal volcanic rocks along with associated granitoids are the predominant rock types in the Kotri belt with a minor occurrence of argillaceous and tuffaceous sequence at the base representing the Dargarh Group. The felsic flows are the most dominant rock type in the Kotri region. The Kotri belt is dominantly composed of felsic flows of Bijli rhyolites along with relatively less mafic flows forming the bimodal suite. Though the Dongargarh and Kotri Supergroups are mutually correlated, the distribution of volcanic rocks in these two regions varies. The Dongargarh granite intruded all the formations of Dongargarh and Kotri. The Pitapani volcanics and Bijli rhyolites are spatially and temporally associated in both Dongargarh and Kotri regions. The Dongargarh granite intruded Pitapani volcanics and Bijli rhyolites in both the regions. In the stratigraphic succession of Bastar craton, the age of the basement gneiss has been dated by U-Pb method as 3.5-3.6 Ga (Ghosh, 2004). It is overlain by Amgaon Group which is dated at 3.0 Ga by Rb-Sr method. Rajesh et al. (2009) reported U-Pb age of 3582±4 Ma for the Amagoan group which is present below the Bailadila Group. The Amgaon Group is overlain by Bengpal Group and the granites of this Group gave an age of 2.5-2.6 Ga by Rb-Sr method (c.f. Ramakrishnan and Vaidyanadhan, 2008). The Bengpal Group, overlain by the Bailadila Group, has been dated at 2.4 Ga by Rb-Sr method. Stratigraphic relationships near the Dalli-Rajhara area reveal that the Bailadila succession is unconformably overlain by the Kotri volcanics/Bijli Rhyolite. $^{207}Pb/^{206}Pb$ SHRIMP zircon ages of 2.7-2.45 Ga and 2450 Ma have been constrained for the Bailadila Group and the Kotri

volcanics respectively (Mukhopadhyay et al., 2012). U-Pb zircon dating has yielded an age of ~2530 for the Bijli rhyolite (Ghosh, 2004). Earlier workers have proposed different models for the generation of the Kotri volcanics. According to Neogi et al., (1996) and Ghosh and Pillay (2012), the Dongargarh volcanics were formed in a rift environment but the associated sediments were formed in a stable continental margin. Asthana et al. (1997) and Rai et al. (2012) proposed that the Dongargarh volcanics with LILE, LREE enrichment and HFSE depletion were generated in an island arc setting. U-Pb zircon geochronology yielded an age of 2432 Ma for the Dongargarh granite (Ahmad et al., 2008) which is correlated with the Malanjkhand granite of 2478 ± 9 and 2477 ± 10 Ma (Panigrahi et al., 2002). Sensarma and Palme (2013) dated the emplacement of Mangikhuta andesite at ~2500 Ma.

In this study, we report the U-Pb zircon geochronology, Lu-Hf isotopic systematic and whole rock major, trace and rare earth element geochemistry of Pitapani mafic volcanic rocks, Bijli rhyolites and Dongargarh granites of Nandagaon Group exposed in the Kotri region. This is the first precise age data on the mafic volcanic rocks along with Bijli rhyolites and Dongargarh granites. Based on the results, we evaluate the role of Palo-Mesoarchean crust through Lu-Hf isotopic signatures to gain insights into the tectono-magmatic episodes and the implications for Neoarchean-Paleoproterozoic crustal growth in the Central Indian Bastar Craton.

2. Geological setting

Central India consists of Archaean to Paleoproterozoic cratonic rocks, mobile belts, Neoproterozoic sedimentary basins, Cretaceous-Tertiary Gondwana sediments and Deccan traps that are classified into Northern Crustal Province (NCP) and Southern Crustal Province (SCP) which are separated by ENE-WSW shear zone (Shivakumar et al., 2003). The Precambrian crust of Central India as preserved in Bastar and Bundelkhand cratons are

accreted in the northern and southern parts of Central Indian Tectonic Zone (CITZ; Roy and Prasad, 2001, 2003; Ramachandra and Roy, 1998, 2012; Roy and Ramachandra, 2012). The Bastar Craton of Central India consists of cratonic components representing the geological events spanning from Mesoarchean to Neoproterozoic in age. It is surrounded by tectonic belts of various ages but its interior has different terranes that were accreted from Paleoarchean to Paleoproterozoic (Fig. 1) which includes the Bengpal-Sukma belt in the south, the Kotri-Dongargarh belt in the center and north, the Amgaon belt in the west, the Sausar-Chilpi belt in the north and the Sonakhan belt in the east. Based on lithological and structural studies, the Sukma (3.0 Ga) and Bengpal Groups (2.6-2.5 Ga) are considered as the oldest Groups (Ramakrishnan and Vaidyanadhnan, 2008). The older TTG gneisses along with younger granitoids have the supracrustals that are included in the Sukma and Amgaon Groups which are metamorphosed to medium to high grade (Ramakrishnan, 1990; Ramachandran et al., 2001). The supracrustals consist of quartzite, pelite, carbonate-BIF association and amphibolites that are intruded by mafic layered complexes. One of the most prominent features at the central part of Bastar Craton is the N-S trending Kotri-Dongargarh belt which is dominated by thick sequence of volcano-sedimentary rocks. The Kotri Supergroup developed over a basement consisting of older TTG and granites that contain Sukma and Bengpal Group of supracrustal affinity and the Bailadila Group of iron formations. The gneisses and the supracrustals are intruded by NW-SE trending mafic dykes (Shivakumar et al., 2012). The volcano-sedimentary sequences in the N-S trending Kotri lineament extends 250 km from Abhujmar basin in the south and up to Sausar belt in the north. The Kotri Supergroup starts with Dargarh Group consisting of bimodal volcanic rocks along with minor tuffs and the sedimentary rocks include grits, sandstones and shales. The overlying Nandgaon Group consists of alternate mafic and felsic flows and pyroclastics. The mafic rocks are basalts and basaltic andesites (Fig. 2A) whereas the felsic rocks are mainly

rhyolite porphyries, rhyolites (Fig. 2B) and minor tuffs (Shivakumar et al., 2012). The rhyolites show prominent development of flow structures distinguished in the field (Fig. 2C). The Nandgaon Group is overlain by alternating volcano-sedimentary sequences of Khairagarh Group (Shivakumar et al., 2003). An unconformity separates the lower Nandgaon and upper Khairagarh Groups. All these rocks are metamorphosed to greenschist to lower amphibolite grade. These volcanic rocks are intruded by the Dongargarh granite (Fig. 2D). Based on petrological and geochemical studies, Krishnamurthy et al. (1990) suggested a comagmatic nature of Dongargarh granites and volcanic rocks of Dongargarh belt. The rocks of this belt have been intruded by pyroxenite-gabbroic anorthosite dykes. U-Pb zircon dates of Bijli rhyolites gave an age of 2491±28 Ma, whereas the Dongargarh granites are dated as 2432±6 Ma (Ahmad et al., 2008; Asthana et al., 2014). However, variable ages of Dongargarh granites overlap the age of Bijli rhyolites (Asthana et al., 2014). Sarkar et al. (1994) noted the geochemical similarity between the rhyolites and granites of Dongargarh Group. Based on structural parameters and metamorphic conditions, Shivakumar et al. (2003) suggested near contemporaneous relationship between the granitoids and lower amphibolite sequence of the Nandagaon Group. In this study, we focus on the mafic and felsic rocks along with associated granitoids from Nandagaon Formation of Kotri belt to evaluate their age, role of ancient crustal component in their genesis and geodynamic setting.

3. Sampling and analytical techniques

3.1 Whole rock geochemistry

The studied samples were been collected from fresh outcrops and quarries which are away from shear zones and devoid of quartz and carbonate veins. Eighteen samples of mafic, thirty six samples of felsic volcanic rocks and eleven samples of granitoids were analyzed for major elements at National Geophysical Research Institute (NGRI) by using the pressed

pellets on XRF (Phillips Magic PRO 1400). JB-2, BHVO-1, JR-1, JA-1, JG-2 and MRG-1 have been used as international reference materials for basalts, rhyolites and granites. Trace and rare earth elements have been analyzed for the same set of samples by High Resolution Inductively Coupled Mass Spectrometry (HR ICP-MS; Nu Instruments Attom, U.K.). Precision and accuracy are referred to Manikyamba et al. (2014a, 2015).

3.2 Geochronology

Zircon grains were separated from crushed fresh rock samples by using gravimetric and magmatic separation method and hand picking under a binocular microscope at the Yu'neng Geological and Mineral Separation Survey Center, Langfang, China. The zircon grains were mounted in epoxy resin disks along with the standard TEMORA1 (417 Ma; Black et al., 2004). The mount was polished, cleaned and then coated by high-purity gold sputter. In order to investigate the internal structures of zircons, cathodoluminescence (CL) images were obtained using scanning electron microscope (JSM510) equipped with Gantan CL probe at the Beijing Geoanalysis Centre, and transmitted and reflected light images were examined by a petrological microscope.

Zircon U-Pb isotopic and trace element analyses were conducted by a laser ablation inductively coupled plasma spectrometry (LA-ICP-MS) housed at the State Key Laboratory of Continental Dynamics of Northwest University, China. On an Agilent 7500a ICP-MS instrument, the laser spot diameter and frequency was set to be 30 μm and 10 Hz, respectively. Harvard zircon 91500 was used as external standard with a recommended $^{206}Pb/^{238}U$ age of 1065.4±0.6 Ma (Wiedenbeck et al., 2004) to correct instrumental mass bias and depth-dependent elemental and isotopic fractionation, the standard silicate glass NIST 610 and GJ-1 were used to optimize the instrument. U-Th-Pb concentrations were calibrated by using NIST 610 as an external standard and ^{29}Si as an internal standard. The

detailed analytical procedures are same with those described in Yuan et al. (2004). The isotopic ratios and ages of $^{207}Pb/^{206}Pb$, $^{206}Pb/^{238}U$, $^{207}Pb/^{235}U$ were calculated using the GLITTER program, and the concordia diagram and weighted mean calculation were computed by using ISOPLOT software (Ludwig, 2003).

In situ zircon Hf isotopic analyses were carried out on the same or adjacent domains of the grains from where the U-Pb dating was done. The analyses were performed on a Nu Plasma HR multiple collector (MC)-ICP-MS instrument at the State Key Laboratory of Continental Dynamics of Northwest University, China. The detailed analytical procedures were the same as those described by Yuan et al. (2008). The energy density of laser ablation and beam diameter used was 15-20 J/cm^2 and 45 μm, respectively. Helium was used as the carrier gas in the ablation cell. Zircon MON-1, GJ-1 and 91500 was used as the reference standard. Recommended $^{176}Lu/^{175}Lu$ ratio of 0.02669 (DeBievre and Taylor, 1993) was used to calculate $^{176}Lu/^{177}Hf$ ratios, and the $^{176}Yb/^{172}Yb$ ratio of 0.5886 (Chu et al., 2002) was used to calculate mean βYb value from ^{172}Yb and ^{173}Yb. Calculation of initial $^{176}Hf/^{177}Hf$ was based on the reference to the chondritic reservoir (Blichert-Toft and Albarède, 1997). Hf model age (T_{DM}) was calculated with respect to the depleted mantle with present-day $^{176}Hf/^{177}Hf = 0.28325$ and $^{176}Lu/^{177}Hf = 0.0384$ (Griffin et al., 2000), and two-stage Hf model age (T_{DM}^{C}) was calculated with respect to the average continental crust with a $^{176}Lu/^{177}Hf$ ratio of 0.015 (Griffin et al., 2002), using the ^{176}Lu decay constant of 1.865×10^{-11} year^{-1} (Scherer et al., 2001).

4. Petrography

The mafic rocks from Kotri belt are primarily composed of varying proportions of clinopyroxene and plagioclase and generally show intergranular texture with occasional porphyritic and spherulitic texture (Fig. 3A). Pyroxene and plagioclase are the dominant minerals embedded in the groundmass consisting of plagioclase, clinopyroxene, amphibole,

chlorite±Fe-oxides. The plagioclase feldspars in the groundmass are elongated to tabular in appearance. Although original igneous textures are retained, at some places these have been transformed into metamorphic mineral assemblages (Fig. 3B). Amphiboles, especially actinolite-tremolite and chlorites occur as the alteration products of Cpx reflecting greenschist to amphibolite facies metamorphism.

The felsic volcanic rocks from Kotri belt are porphyritic in nature, and consist of alkali feldspar, quartz, plagioclase as essential minerals; biotite, zircon and opaque minerals occur as accessory phases. The K-feldspar, quartz and plagioclase phenocrysts are embedded in a siliceous, merocrystalline groundmass of quartz, K-feldspar, tiny flakes of biotite, opaque and glass. Some of the K-feldspars are perthitic showing fine exsolution lamellae of plagioclase within the host K-feldspar (Fig. 3C). Compositionally, plagioclase grains are albitic with very low An content (An_6 to An_8; determined by X'^ 010 symmetric extinction angle). Some of the plagioclase crystals are saussuritized. K-feldspar and plagioclase grains contain inclusions of tiny biotite and opaques. In most of these rocks primary igneous flow texture is retained in the groundmass whereas rotational porphyroblasts of K-feldspar implies the syntectonic rotation of the grains (Fig. 3D).

The Kotri porphyritic granitoids are characterized by the development of pink to white colored K-feldspar phenocrysts (ranging up to 4 cm in length) which occur as prismatic grains along with microcline and lath-shaped plagioclase. Perthite occurs in both flame and string varieties (Fig. 3E) showing well developed exsolution lamellae. Anorthite content of plagioclase varies from An_{17} to An_{24} (determined by X'^ 010 symmetric extinction angle) corresponding to oligoclase variety. Groundmass is mainly quartz, microcline, plagioclase and biotite. Most of the biotite grains are showing their strong pleochroic green colour possibly due to Fe enrichment. Accessory minerals include zircon, apatite and opaque grains formed at the expense of biotite and sphene. Large phenocrysts of microcline and plagioclase

are embedded in a groundmass of quartz, feldspar and biotite representing porphyritic texture. In some places, vermicular intergrowth of quartz within alkali feldspar is observed depicting graphic texture (Fig. 3F). Saussuritization of plagioclase is a common feature in these granitoids.

5. Geochemistry

5.1 Effects of alteration and element mobility

The primary geochemical signatures of volcanic rocks from Archean terranes are overprinted by several geological processes including polyphase deformations, post-depositional tectonothermal events, late stage intrusions, hydrothermal activity, metamorphism, metasomatic alterations and carbonations leading to redistribution of elements (Frei et al., 2002; Polat and Hofmann, 2003). However, behavior of major and trace elements that are resistant to metamorphic and hydrothermal alteration processes and remain immobile provide essential parameters to decipher the source characteristics, petrogenetic and tectonic implications for mantle-derived magmas (Arndt et al., 1989; Lesher and Arndt, 1995; Lesher et al., 2001; Song et al., 2006). Studies on effects of alteration on element mobility and geochemical patterns of Archean igneous suites have suggested that selected major elements (Al, Ti, Fe, and P), high field strength elements (HFSE; Y, Th, Nb, Ta, Zr, Hf), the rare earth elements (REE; except Ce, Eu) and transition metals (Cr, Ni, Co, Sc, V) are relatively immobile and remain unaffected during sea floor hydrothermal alteration and metamorphism (Sun and Nesbitt, 1978; Ludden et al., 1982; Jochum et al., 1991; Lafleche et al., 1992; Polat et al., 2002; Munker et al., 2004; Manikyamba et al., 2008; Said and Kerrich, 2009). The HFSE and REE due to their high valencies, electronegativities, small radii and strong chemical bonds are trapped in the structures of secondary minerals when their primary host minerals are destroyed during alteration processes. These elements maintain constant ratios thereby reflecting their immobility during hydrothermal alteration and metamorphism

(Song et al., 2006; Arndt et al., 2008; Said and Kerrich, 2009; Said et al., 2011). In this study, HFSE and REE compositions and their ratios have been considered to evaluate the petrogenetic processes and tectonic setting of the volcanic rocks and granitoids from Kotri. Polat et al. (2002) evaluated the effects of alteration and metamorphism on volcanic rocks of Isua greenstone belt, Greenland and suggested that rocks having LOI > 6 wt. % were subjected to variable alteration. The volcanic rocks and granitoids from Kotri have < 6 wt. % LOI (Table 1) indicating minimum effects of alteration.

5.2 Geochemistry of volcanic rocks

The major, trace and rare earth element data of Kotri volcanic rocks are listed in Table 1. The SiO_2 content of these rocks range from 47 to 76 wt. % in which the mafic and felsic volcanic rocks have SiO_2 content varying from 47-54 wt. % and 67-76 wt. % respectively indicating bimodal composition. Their bimodal nature is also supported by the relationship between SiO_2 and various major elements (Fig. 4) with the Kotri volcanic rocks forming two clusters. The MgO and CaO decreases with increasing SiO_2, indicating the fractional crystallization of olivine and clinopyroxene. Similarly, Al_2O_3, TiO_2, Fe_2O_3 and P_2O_5 decreases from mafic to felsic rocks, whereas Na_2O and K_2O increase with increasing SiO_2, indicating fractional crystallization. On total alkali vs. silica diagram most of the mafic rocks represent the basalts except one basaltic trachy-andesite and one basenite. The felsic rocks fall in the field of rhyolite with a minor spill in dacite and trachy-dacite fields depicting a typical bimodal nature (Fig. 5). The basalts have low TiO_2 (0.4-1.8 wt.%), moderate Al_2O_3 (11.6-14.5 wt.%) and Mg number (Mg#, 30-41) along with low ferromagnesian trace element contents (Co= 30-83 ppm; Cr= 13-56 ppm; Ni= 12-46 ppm). Rhyolites have low CaO (0.6-3.3 wt.%), moderate Al_2O_3 (9.69-12.18 wt.%) and relatively high total alkali content (6.64-10.29wt.%) with very low ferromagnesian trace element contents (Co= 0.2-2.3 ppm; Cr= 0.3-

5.2 ppm and Ni= 0.2-1.7 ppm). Primitive mantle normalized basalts and rhyolites exhibit distinct negative anomalies for Nb-Ta and Ti with relative enrichment in Th and La (Fig. 6A, C). Basalts are slightly fractionated except one sample which shows a flat pattern in chondrite normalized REE diagram ($(La/Yb)_N$=1.26-8.92) with feeble Eu anomaly (Eu/Eu*=0.72-0.94). In contrast, the rhyolites have strongly fractionated patterns ($(La/Yb)_N$= 11.2-15.3) with significant negative Eu anomaly (Eu/Eu*=0.20-0.88) (Fig. 6B, D).

5.3 Geochemistry of granitoids

The granitoids show high SiO_2 (69-78 wt.%) and K_2O (6.3 - 7.4 wt. %) and Na_2O (2.8 - 3.7 wt. %) with molar $Al_2O_3/CaO+Na_2O+K_2O$ (A/CNK) ranging from 0.92 - 1.13 and are classified as potassic granites (Table 2). They have high Fe∗[FeOt/(FeOt + MgO)] varying from 1.6 to 3.1 and are further classified as ferroan granites with Na_2O+K_2O/Al_2O_3 (NA/K) > 0.85 indicating their alkaline nature (Whalen et al., 1987). On the normative An-Ab-Or diagram the analysed granitoids are occupying the field of granites (Barker, 1979; Fig. 7A). These granites have distinctly high concentrations of Ba, Rb and Zr; and low Sr, Y and transitional elements. On primitive mantle normalized diagram (Fig. 7B) they display Th enrichment with significant negative Nb, Ta and Zr anomalies. Their chondrite normalized REE patters are highly fractionated ($(La/Yb)_N$= 12.9-22.2) with distinct negative Eu anomaly (Fig. 7C).

6. Zircon geochronology

6.1 U-Pb isotopes

Mafic volcanic rocks

Zircons in sample KB-55 are colorless or light brown and translucent. The anhedral to subhedral grains show near-prismatic or irregular morphology with lengths of 50-200 μm and length to width ratios varying from 2:1 to 1:1. In CL images, most zircon grains show clear oscillatory zoning, and few grains show thin bright overgrowth rims (Fig. 8). Thirty one spots were analyzed on thirty one zircon grains from this sample. The analytical results are listed in Table 3 and plotted in the Concordia diagram (Fig. 9A). The analytical data show a wide range of Pb (50-221 ppm), U (94-402 ppm) and Th (11-210 ppm) with Th/U ratios of 0.06-0.66 (with an exception of one spot 0.06). All the spots cluster as a coherent group on the concordia (concordance of 95-100%) with $^{207}Pb/^{206}Pb$ spot ages ranging from 2446 to 2522 Ma. The data yield $^{207}Pb/^{206}Pb$ weighted mean age of 2471±7 Ma (Fig. 8A; MSWD = 0.6) and suggesting early Paleoproterozoic magmatic event.

Felsic volcanic rocks

Zircons in sample KB-26 are colorless or light brown, and transparent to translucent. The subhedral to euhedral grains show near-spherical or prismatic morphology with lengths of 40-200 μm and length to width ratios vary from 2:1 to 1:1. Most grains show clear oscillatory zoning with some heterogeneous fractured domains (Fig. 8). A total of 29 spots from 29 zircons were analyzed from this rock and the results show Pb, U and Th contents in the range of 57-253 ppm, 111-494 ppm and 7-284 ppm respectively, with Th/U ratio varying from 0.36 to 0.70 (with one exception of 0.06; Table 3) . The data define an upper intercept age of 2479±13 Ma (Fig. 9B; MSWD = 1.5) which is considered to represent the magmatic event during early Paleoproterozoic.

Zircons in sample KB-35 are light brown, transparent to translucent. The euhedral to subhedral grains show near-spherical or near-prismatic morphology with lengths of 30-200 μm and length to width ratios vary from 2.5:1 to 1:1. In CL images, most zircons show clear

oscillatory zoning (Fig. 8). A total of 32 spots from 32 zircons were analyzed from this rock (KB-35; Table 3) and the results show high Pb content of 119 - 302 ppm, U content of 200-572 ppm and Th content of 22-418 ppm with Th/U ratios varying between 0.06-0.73. The data define an upper intercept age of 2463±14 Ma (Fig. 9C; MSWD = 0.54). Based on these results, 2463±14 Ma is interpreted to represent magmatic crystallization event during Paleoproterozoic.

Granites

The zircon grains in sample KB-127A are translucent and colorless. Most of the grains are subhedral to euhedral, displaying near prismatic features with lengths ranging from 30 to 200 μm and aspect ratios vary from 2:1 to 1:1. In CL images, the zircon grains show clear oscillatory zoning (Fig. 8). A total of 25 spots from 25 zircons were analyzed from this rock and the results show high Pb, U and Th contents in the range of 45-351 ppm, 77-740 ppm (even up to 1471 ppm) and 40-637 ppm with Th/U ratio varying from 0.32-0.66 with one spot showing lower value of 0.06). The data define an upper intercept age of 2506±50 Ma (Fig. 9D; MSWD = 3.0) suggesting latest Neoarchean magmatic crystallization event.

6.2 Lu-Hf Isotopes

A total of 38 zircon grains were analyzed for Lu-Hf isotopes on the same domains from where the U-Pb age data were estimated. The results are presented in Table 4 and plotted in Fig. 10. The Lu-Hf data on zircons from the individual rock types are briefly discussed below.

Eight zircon grains were analyzed from sample KB-55 for Lu-Hf isotopes. The result shows initial $^{176}Hf/^{177}Hf$ ratios range from 0.280925 to 0.281018. The $\varepsilon_{Hf}(t)$ values are in the range of -10.0 to -6.7. The Hf depleted model ages (T_{DM}) are between 3038 Ma and 3171 Ma,

and Hf crustal model ages (T_{DM}^{C}) varies from 3387-3589 Ma. The predominant negative $\varepsilon_{Hf}(t)$ values suggest that the source material was evolved from the Paleoarchean crust. Ten zircons were analyzed from sample KB-26 for Lu-Hf isotopes. The result shows initial $^{176}Hf/^{177}Hf$ ratios range from 0.280919 to 0.281020. The $\varepsilon_{Hf}(t)$ values are varying from -10 to -6.4. The Hf depleted model ages (T_{DM}) are between 3038 Ma and 3182 Ma, and Hf crustal model ages (T_{DM}^{C}) varies from 3377-3596 Ma. Ten zircons were analyzed from sample KB-35 for Lu-Hf isotopes. The result shows initial $^{176}Hf/^{177}Hf$ ratios range from 0.281000 to 0.281103. The $\varepsilon_{Hf}(t)$ values are in the range of -7.5 to -3.9. The Hf depleted model ages (T_{DM}) are between 2925 Ma and 3072 Ma, and Hf crustal model ages (T_{DM}^{C}) varies from 3208-3432 Ma. The predominant negative $\varepsilon_{Hf}(t)$ values of these samples suggest that the source material was evolved from the Paleoarchean crust.

Ten zircons were analyzed from sample KB-127A for Lu-Hf isotopes. The result shows initial $^{176}Hf/^{177}Hf$ ratios range from 0.280937 to 0.281062. The $\varepsilon_{Hf}(t)$ values are in the range of -8.8 to -4.3. The Hf depleted model ages (T_{DM}) are between 2979 Ma and 3170 Ma, and Hf crustal model ages (T_{DM}^{C}) varies from 3269-3541 Ma. The predominant negative $\varepsilon_{Hf}(t)$ values also suggest that the source material was evolved from the Paleoarchean crust.

7. Discussion

7.1 Petrogenesis of mafic rocks

The basalts of the Kotri belt are characterized by low Mg# (30-41) Ni (<46 ppm), Cr (<56 ppm), Co (<83 ppm) contents compared to primary basaltic magmas from the mantle (Wilson, 1989) suggesting their derivation through fractionation of Si-poor mafic phases such as olivine, clinopyroxene and Fe-Ti oxides, either in the magma chamber of their parental magma or *en route* to the surface (Huppert and Sparks, 1985; Wilson, 1989; Lesher et al., 1999). This is consistent with the presence of clinopyroxene as the dominant phenocrysts and

the negative correlations of MgO, Fe_2O_3, TiO_2 and CaO contents against SiO_2 (Fig. 4). These rocks with higher Zr/Nb ratios (15-166; Table 1) than that of ocean island basalt (OIB, 5.83), suggest that they were not derived from OIB-like asthenospheric mantle. In addition, none of the geochemical characteristics of these basalts are comparable to mid-ocean ridge basalt (MORB)-type mantle. The Kotri basalts exhibit arc-related magmatic affinities with negative Nb-Ta anomalies coupled with LREE and LILE enrichment with respect to the HFSE (Fig. 6A). The subduction zone affinity is also evident from LILE fractionation which resulted in high inter-element ratios such as Ba/Nb (12-1104, av.170), Ba/La (8-308, av.33) and La/Nb (1-32, av.5). Based on their Nb-Ta anomalies, LILE and LREE enrichment; it is suggested that arc magmatism played an important role in the generation of these basalts. On Nb/Yb vs. Th/Yb plot (Fig. 11A), Kotri basalts plot above the MORB-OIB array (Pearce, 2008; Pearce and Peate, 1995) in the arc field. Schiano et al. (1995) reported the enrichment of depleted mantle sources by slab-derived magmas based on the study of melt inclusions in olivines from mantle xenoliths in arc-related magmatic provinces. This process may be analogous to those reported from the mafic rocks in the Mariana Trough (Volpe et al. 1987), the Brevenne metamafic rocks from the Massif Central, France (Pin and Paquette, 1997), the Mid-Atlantic Ridge asthenospheric mantle (le Roux et al. 2002), the Far Eastern Russian mantle xenoliths (Yamamoto et al., 2004), and the Jurassic island-arc magmatism in the eastern Rhodope Massif (Bulgaria, Bonev and Stampfli, 2008).

In general, low La/Yb ratios reflect a melting regime dominated by relatively larger degrees of melting and/or spinel as the predominant residual phase, whereas high La/Yb ratios are indicative of smaller degrees of melting and/or garnet melting regime (Yang et al., 2007). The high $(La/Sm)_N$ (1.07-3.47) and $(Tb/Yb)_N$ (1.11-1.39) ratios, in combination with flat MREE to HREE patterns (Fig. 6B) for the Kotri basalts, suggest that they were generated by relatively lower degrees of partial melting of a mantle source in the spinel-peridotite

melting regime, translating to depths shallower than 60-70 km (Fig. 11B). Further, the $\varepsilon_{Hf}(t)$ values in the mafic rocks and the corresponding T_{DM} and T_{DM}^{C} values vary between -10.0 and -6.7, 3038 and 3171 Ma, and 3387 and 3589 Ma respectively. The predominant negative $\varepsilon_{Hf}(t)$ values suggest that the source material was evolved from the Paleoarchean crust which is consistent with the observation of Mishra et al. (1988) that the Kotri rocks were developed on a sialic crust comprising older TTG and granites. The LILE and LREE enrichment in these basalts are due to the involvement of subduction components/crustal input. Therefore, in summary, the Kotri mafic rocks are interpreted to have been derived from an incompatible elements enriched, subduction-modified lithospheric mantle, and experienced olivine + clinopyroxene fractionation with minor upper crustal contamination. Nb/Th ratio range from 0.16-4.13 (Nb/Th of continental crust is ~2.6) also supports crustal signatures for the generation of Kotri basalts.

7.2 Petrogenesis of felsic rocks

Several processes including liquid immiscibility, partial melting and fractional crystallization have been proposed for the formation of felsic rocks in bimodal suites (Bonnefoi et al., 1995; Freundt-Malecha and Schmincke, 2001). The segregation of an immiscible silicate liquid after extensive differentiation of Fe-rich basalts has been proposed for the production of oceanic plagiogranites (Dixon and Rutherford, 1979). However, the experimental studies of Ryerson and Hess (1978) and Watson (1979) on co-existing mafic and felsic melts indicate that several trace elements including REE are strongly partitioned into the mafic liquid leaving the felsic melt depleted in these elements. Peccerillo et al. (2003) developed a method to discriminate between crustal melting and fractional crystallization (FC) models using compatible elements.

Basalts and felsic lavas erupted penecontemporaneously with the felsic lavas that are stratigraphically younger and have similar Nb/Th values, trace and rare earth element characteristics probably sharing a common mantle-derived primary magma, as demonstrated for volcanic series of oceanic (Geist et al., 1995) and continental (Nono et al., 1994) intraplate domains. Similarly, the Kotri bimodal volcanic suite is considered as co-magmatic, despite a large gap in their major elements chemistry. Although similar major and trace element variations (Fig. 4) can result from magma mixing/mingling, kinked trends and pronounced compositional gaps argue against this and instead favor fractional crystallization and assimilation. In contrast to the Harker diagram, the relationship between HFSE and REE ratio (Figure not shown; Langmuir et al., 1978) lack a compositional gap and display a linear trend, pointing to a genetic link between the mafic and felsic rocks and the role of crustal assimilation during the petrogenesis of Kotri volcanics. This is consistent with the active continental margin nature of the Kotri felsic volcanic rocks (Figs. 11A, C) which suggests that subduction-related signatures were inherited from their mafic counterpart.

The felsic rocks of Kotri volcanics have wide ranges in major and trace element contents (e.g., SiO_2 = 67-76 wt.%) that can be explained by crystal fractionation. The negative correlations of CaO, Al_2O_3, Fe_2O_3 and TiO_2 versus SiO_2 (Fig. 4) indicate the fractionation of amphibole±plagioclase±Fe-Ti oxides. The pronounced negative Eu anomalies in the chondrite normalized REE patterns of the felsic rocks suggest a significant amount of plagioclase fractionation. Simple fractional crystallization of mafic parental magma to produce the felsic magmas, however, is inconsistent with the lack of intermediate compositions. Instead, it requires some special conditions to explain the wide compositional gap (e.g. SiO_2 = 47-54 to 67-76 wt. %) in the Kotri volcanics. Such compositional gap may have developed in magma chamber due to the sensitivity of the rheology to crystal content (i.e., critical crystallinities) and the magmatic silica content, which collectively control the

relative rates of crystal settling and crystal retention (Pe-Piper and Moulton, 2008; Deering et al., 2011; Rooney et al., 2012). Therefore, it is suggested that FC of the associated basalt involving clinopyroxene, biotite, plagioclase and Fe-Ti oxide generated the Kotri felsic rocks.

Further, the Kotri mafic volcanic rocks have a total REE abundance of 43-230 ppm (av. 146 ppm) whereas the felsic rocks have 283-561 ppm (av. 386 ppm). The pronounced enrichment of the REE in felsic rocks relative to mafic rocks suggests that liquid immiscibility cannot account for the petrogenesis of the Kotri volcanic suite. The rhyolites are characterized by REE patterns with prominent negative Eu anomaly (Fig. 6D) indicating the fractional crystallization of plagioclase (Rollinson, 1993). Plagioclase fractionation is also supported by the negative correlation between SiO_2, CaO (r^2 = -0.78) and Al_2O_3 (r^2 = -0.79) in the rhyolites (Fig. 4). The felsic rocks display fractionated REE patterns with pronounced LREE enrichment and depletion of MREE relative to the HREE (Fig. 6D), which are attributed to fractionation of clinopyroxene and hornblende (Morata et al., 2000; Rollinson, 1993). The fractionation of basaltic melt should ideally produce a continuum of compositions from unfractionated basalt through intermediate compositions to rhyolite (Best and Christiansen, 2001). In case of Kotri volcanics, the rocks are basaltic and rhyolitic without any intermediate variety of andesitic composition. Peccerillo et al. (2003) suggested that the mass of residual liquids during fractional crystallization from basalts to rhyolites does not change linearly with falling temperature, rather it decreases slowly during the early stage and drops abruptly through the intermediate to final stages of fractional crystallization. A consequence of this rapid drop of residual liquid mass during the intermediate stage of fractional crystallization is the production of an insignificant amount of intermediate rocks. Thus, we propose the closed-system fractional crystallization as a possible mechanism for the generation of the felsic rocks of Kotri volcanic suite. Further, the high SiO_2 with significant enrichment in LILE and LREE and depletion in HFSE, suggests that primary basaltic magma

was assimilated by continental crust causing crustal anatexis. Moreover, the $\varepsilon_{Hf}(t)$, T_{DM}, T_{DM}^{C} values varying from -10 to -6.4, 3038 Ma to 3182 Ma, and 3377 to 3596 Ma are consistent with the evolution of source material from the Paleoarchean sialic crust comprising older TTG and granites.

The occurrences of rhyolites in intraoceanic arc, continental arc and continental rift settings and their geochemical features are attributed to different petrogenetic processes (Ayalew and Ishiwatari, 2011). Rhyolitic magmas in island arcs are derived by dehydration melting of calc-alkaline andesites in upper to middle oceanic arc crust (Tamura and Tatsumi, 2002), whereas continental arc rhyolites are products of partial melting of metamorphosed basalts of thickened lower crust associated with fractional crystallization and crustal assimilation (Deering et al., 2008). Fractional crystallization and crustal contamination of basaltic magma derived by intracrustal melting account for the origin of continental rift zone rhyolites (Garland et al., 1997). On the basis of their geochemical signature, rhyolites are classified as FI (calc-alkaline, low HFSE, moderate to high Zr/Y, La/Yb_n: 5.8-34, strong subduction signatures), FII (calc-alkaline to transitional, intermediate HFSE, moderate Zr/Y, La/Yb_n: 1.7-8.8; prominent subduction signatures), FIIIa (tholeiitic, moderate HFSE, low Zr/Y, La/Yb_n: 1.5-3.5, weak subduction signatures) and FIIIb (tholeiitic, high HFSE and HREE, low Zr/Y, La/Yb_n: 1.1-4.9, no subduction signatures) types (Lesher et al., 1986; Manikyamba et al., 2014b). The geochemical characteristics of Kotri rhyolites marked by high-silica, moderate Al_2O_3, moderate to high alkali contents, moderate potassic character, low ferromagnesian trace element (Ni, Co, Cr) contents, Th, La, Zr enrichment, higher Yb contents, strongly fractionated LREE/HREE patterns and pronounced negative Eu (Eu/Eu*=0.20-0.88) and Ti anomalies primarily classify them as FI type rhyolites. Further, their alkaline composition, LILE-LREE enrichment, relative depletion in HFSE contents, moderate to high Zr/Y values (1.5-8.3), La/Yb_n ranging from 11.2 to 15.3 and pronounced

negative Eu anomalies are comparable with both FI and FII type rhyolites from other Archean greenstone belts (Lesher et al., 1986). The trace and REE chemistry of Kotri rhyolites attests to strong subduction signature in their evolution which in turn, justifies their characterization as FI and FII rhyolite types. FI rhyolites are interpreted to be generated by partial melting of thick basaltic crust metamorphosed to amphibolite/eclogite at ~40 km leaving garnet in the residue. FII types are produced at depths ranging from 10-30 km with amphibole-plagioclase residue. The FI and FII rhyolites of Kotri are thus interpreted to be products of partial melting of thick basaltic crust metamorphosed to amphibolite/eclogite facies at depths ranging from >30 km to 10 km with garnet and amphibole-plagioclase-bearing mantle residue respectively. Felsic volcanic rocks occurring in association with komatiite-tholeiite sequence from the northern Superior Province greenstone belts have been classified as Type 1 and Type 2 (Hollings et al., 1999). Type 1 rhyolites are characterized by relatively aluminous composition and strongly fractionated HREE patterns, whereas Type 2 has flat HREE with elevated Ni and Cr contents. Both Type 1 and Type 2 show LREE enriched patterns and negative Nb and Ti anomalies. Type 3 rhyolites are characterized by moderate LREE fractionation, flat HREE patterns, pronounced negative Eu and Ti anomalies, interpreted as the products of intracrustal fractional crystallization of basaltic liquids. Type 1 rhyolites are generated by oceanic slab melting and Type 2 rhyolites are suggested to be derived through mixing of Type 1 rhyolites with tholeiitic magmas, or a contribution from mantle wedge sources located above the garnet stability field. The Kotri rhyolites showing prominent negative Eu, Ti anomalies, pronounced LREE/HREE fractionation are geochemically akin to Type 3 rhyolites.

7.3 Petrogenesis of granitoids

Generation of A-type granites are explained through various processes such as direct fractionation of products of mantle-derived alkali basalts, partial melting of K-rich basaltic

rocks (Turner et al., 1992; Litvinovsky et al., 2002; Mushkin et al., 2003; Bonin, 2007; Jahn et al., 2009; Eyal et al., 2010), and anatexis of either pre-existing crust (Rämö et al., 1995; Dall'Agnol et al., 2005) or juvenile crust (Frost and Frost, 1997; Frost et al., 1999). Petrogenetic models for A-type magmas have involved either partial melting of specific crustal protoliths (Collins et al., 1982; Creaser et al., 1991; Whalen et al., 1987), or extensive fractional crystallization from mantle-derived basaltic magmas (Turner et al., 1992). Felsic magmas having low HREE (Yb<1.9 ppm) and Y (<18ppm contents) are suggested to be derived by partial melting of basaltic crust of the subducted oceanic lithosphere with garnet remaining as a residual phase (Pearce and Peate, 1995; Defant and Kepezhinskas, 2001). The high HREE (Yb>1.9 ppm) and Y (>18ppm) contents for the Kotri granites (Yb: 4.0-8.5 ppm; Y: 49-107 ppm) suggest origin of parent magma through slab dehydration and shallow level partial melting of mantle wedge where garnet entered the melt phase. Depletion of Sr and marked negative Eu anomalies (Fig. 7B) in these granites therefore require melting of a source rock within the stability field of plagioclase. This implies that the source regions of the Kotri granites are relatively shallow (<30 km). The $\varepsilon_{Hf}(t)$ values of granites are in the range of -8.8 to -4.3 with the Hf depleted model ages (T_{DM}) and Hf crustal model ages (T_{DM}^{C}) varying from 2979 Ma to 3170 Ma and 3269-3541 Ma respectively, suggesting the role of Paleoarchean felsic crustal source in the evolution of granitic magma.

7.4 Age of bimodal volcanism and associated granitoid magmatism in the Kotri belt

Volcanic rocks and associated granites are the dominant components in the Kotri belt. Based on lithostratigraphic relationships and comparisons between volcanic rock associations from adjacent regions, the rock types of Kotri belt are considered to be of Paleoproterozoic in age. The CL images of zircons from these rocks in our study display typical oscillatory growth zoning suggesting a magmatic origin as also supported by their Th/U ratios (0.4).

Therefore, we suggest that the U-Pb ages represent the time of formation of the volcanic rocks. The weighted mean $^{207}Pb/^{206}Pb$ ages for zircons from mafic (2471±7 Ma), and felsic volcanic rocks (2479±13 and 2463±14 Ma) indicate an average age of 2.47 Ga which is consistent with the early Paleoproterozoic magmatism in the Bastar Craton.

The U-Pb zircon ages of Kotri granitoids of present study display an age of 2506±50 Ma suggesting the Neoarchean granitoid magmatism along the Kotri belt. Till date, there is no age data available for the mafic volcanic rock from Kotri-Dongargarn belt (Sensarma and Plame, 2013). The U-Pb single crystal zircon dating of the oldest Bijli rhyolite yield an age of 2530 Ma (Ghosh, 2004). However, Asthana et al. (2014) reported U-Pb age of 2491±28 Ma for the Bijli rhyolite. According to Ahmad et al. (2008), U-Pb age of Dongargarh granite is 2432±6 Ma which is slightly younger than that of Bijli rhyolite dated by Asthana et al. (2014). The intrusive Dongargarh granite is correlated with the well known Cu-Mo-Au bearing Malanjkhand granitoid dated at 2478±9 Ma and 2477±10 Ma (Panigrahi et al., 2002).

The geochronological data reported in this study suggest that Kotri mafic and felsic volcanic rocks were erupted coevally during the Paleoproterozoic time which is almost synchronous with the granitoid magmatism during Archean-Proterozoic transition in the Bastar Craton. The felsic volcanic rocks are equivalent with the overall age of Bijli rhyolite emplaced within the Dongargarh granite. This coeval age is also equivalent with U-Pb zircon age of Malanjkhand granite. The available Re-Os ages of molybdenites also show similar age of ~2500 Ma (Stein et al., 2004). Based on the present geochronological data it is suggested that this entire bimodal volcanism and granitoid magmatism are representative of Central Indian tectonothermal event within the Kotri-Dongargarh tectonic window during Archean-Proterozoic time frame.

7.5 Geodynamic setting

Bimodal volcanism typically characterizes an extensional environment which can occur at various tectonic settings, such as continental rifts (Duncan et al., 1984; Garland et al., 1995; Pin and Marini, 1993), oceanic islands (Frey et al., 1984; Pin and Paquette, 1997), island arcs (Frey et al., 1984; Hochstaedter et al., 1990), back-arcs (Hochstaedter et al., 1990; Pearce et al., 1995, 1999; Elliott et al., 1997; Ewart et al., 1998; Shinjo and Kato, 2000) and within-plate environment (Frost et al., 1999; Bonin, 2004). Bimodal magmatic rocks from these various settings usually display distinct geochemical characteristics and diagnostic relationships between their mafic and felsic end members (Pin and Paquette, 1997; Wang et al., 2000). For example, continental rift bimodal volcanic rocks typically consist of abundant felsic and minor mafic rocks with similar geochemical characteristics, such as high-K and enrichment in LILEs and HFSEs (Duncan et al., 1984; Pin and Marini, 1993; Garland et al., 1995). Bimodal volcanic rocks from oceanic island settings consist of voluminous mafic and subordinate felsic rocks with low-K and depletion in incompatible elements (Ikeda and Yuasa, 1989). The mafic and felsic rocks in island arc and back-arc settings are characterized by enrichment in LILEs and LREEs, depletion in HFSEs (Frey et al., 1984; Hochstaedter et al., 1990; Pin and Paquette, 1997). In contrast, the mafic rocks from within-plate settings are typically tholeiitic gabbros and/or basalts, whereas the coeval felsic rocks generally display the geochemical characteristics of A-type granites (Turner et al., 1992; Frost et al., 1999; Bonin, 2004).

The LILE enrichment and HFSE and HREE depletion in the Kotri basalts suggest that they were generated in a subduction zone setting (Wilson, 1989) where the mantle source was depleted in HFSE and enriched in LILEs through subduction related processes which is also supported by negative $\varepsilon_{Hf}(t)$ values (Wilson, 1989; Marlina and John, 1999; Stern, 2002). These characteristics are similar to those of the basalts from island arc and back-arc settings,

but differ from continental rift, oceanic island and within plate basalts (Pearce, 1982; Ikeda and Yuasa, 1989; Fretdorff et al., 2002). Woodhead et al. (1993) and Gamble et al. (1995) compared island-arc and back-arc basalts, and suggested that the latter are characterized by relatively high Ti, V, Zr, and Nb contents. The Nb content for island-arc basalts is usually less than 2 ppm (Pearce et al., 1995, 1999; Elliott et al., 1997; Ewart et al., 1998). In contrast, the Nb contents (3.5-10.8 ppm) of Kotri mafic volcanic rocks are much higher than those of island-arc basalts, and their average Ti, V and Zr contents (1.21 wt.%; 221 ppm; 171 ppm) are similar to those of back-arc basalts (Woodhead et al., 1993; Gamble et al., 1995; Pearce et al., 1995, 1999; Shinjo and Kato, 2000). These lines of evidence suggest that the lithospheric mantle was metasomatized by slab-derived fluids (Kepezhinskas et al., 1996; Sajona et al., 1996; Petrone and Ferrari, 2008) and the partial melting of the lithospheric mantle occurred in a back-arc extensional environment triggered by thermal erosion through rising hot asthenosphere (Gilder et al., 1991; Ren et al., 2002). This interpretation coupled with the arc signatures of the felsic rocks as mentioned above is consistent with the inference that bimodal suites are usually developed in extensional tectonic settings (Coward et al., 1987).

On the basis of Zr vs 10,000*Ga/Al plot (Fig. 12A; Whalen et al., 1987) the granites indicate A-type characteristics. It has long been recognized that A-type magmas are formed in a variety of extensional regimes, from continental arc to back-arc extension to post-collisional extension and within-plate settings (Eby, 1992, Forster et al., 1997, Whalen et al., 1996). The relationship between Rb, Y and Nb indicate within-plate tectonic setting for the generation of Kotri granites (Fig 12B). The associated bimodal volcanic rocks of Kotri belt have back-arc basin affinity with predominant negative $\varepsilon_{Hf}(t)$ values suggesting the role of Paleoarchean crust in the generation of granitic source magma. Considering these observations, we suggest that the A-type granites of Kotri belt are likely to have been emplaced at the terminal stage of continental arc, most probably at the beginning stage of the

extension of back-arc or of the rifting of continental arc. The shallow depth of melting for the Kotri granites is consistent with this extensional tectonic regime. The upwelling of asthenosphere as a consequence of back-arc extension or intra-arc rift triggered the partial melting of the amphibolitized Archaean metamorphic basement (including metasedimentary and metaigneous rocks) and generated the Kotri A-type granitic magmas. The available geochemical and geochronological data indicate that bimodal volcanic rocks of Kotri belt were erupted at a back-arc setting associated with an active continental margin.

A schematic diagram (Fig. 13) illustrates the tectonic environment that facilitated synchronous, bimodal volcanism of the Bijli rhyolites and Pitapani basalts of Kotri-Dongargarh orogen. The HFSE composition of the FI-FII/Type 3 rhyolites commensurates with intracrustal melting of thickened metamorphosed crust by subduction-derived melts and subsequent fractional crystallization in an active continental margin setting (Fig. 13). The geochemical signatures of the basalts, which erupted contemporaneously with the rhyolites, corroborate a continental back arc setting. In this tectonic regime, rifting at the back arc induced decompression melting of the upwelling asthenospheric mantle that is modified and enriched by subduction processes operating in the associated arc environment. Melts derived from this asthenospheric melting ascended through continental lithosphere, assimilated older crust and erupted as basalts in the back arc rift setting (Fig. 13). Granitoids associated with this bimodal magmatism preserve geochemical signatures of anorogenic, within-plate magmatism reflecting extensive assimilation of crustal materials by parental magmas.

Bulk geochemical, Sr-Nd-Pb isotopic and experimental studies with thermodynamic modelling for bimodal magmatism at the Carlingford Igneous Centre, Ireland (Meade et al., 2014) suggest that the crust is very fusible, but repeated heating events rapidly lower its melt-production capacity. The cessation of partial melting of the crust terminated granitoid magmatism and subsequent melt generation processes involved less fertile restite

compositions resulting into mafic intrusions and a pronounced compositional gap. The phenomenon of 'progressively inhibited crustal assimilation' (PICA) has been proposed as a major trigger for bimodal volcanism in a continental setting (Meade et al., 2014). In the present study, the generation of felsic (active continental margin) and mafic (continental back arc) magmas in two distinct tectonic environments and progressively inhibited crustal assimilation (PICA) ensuing granitoid emplacement are invoked as viable causes that restricted generation of magmas with intermediate compositions thereby promoting bimodality in contemporaneous mafic-felsic magmatism in Kotri.

8. Conclusions

- The Kotri belt contains a bimodal basalt-rhyolite association and granites which are suggested to have been generated in an extensional environment similar to a back arc basin.
- The zircon U-Pb age data on the mafic volcanic rocks is 2471±7 Ma and the felsic volcanic rocks 2479±13 and 2463±14 Ma indicate the Paleoproterozoic bimodal volcanic activity in the Kotri belt.
- The U-Pb zircon age of Kotri granitoid is 2506±50 Ma suggesting the granitoid magmatism during Archean-Proterozoic transition.
- The Lu-Hf isotope data suggests that the source material was evolved from the subduction of Paleoarchean sialic crust comprising older TTG and granites. The $\varepsilon_{Hf}(t)$, T_{DM}, TDM^{C} values of granites indicate the role of Paleoarchean felsic crustal source in the evolution of granitic magma.
- The obtained geochronological data for both volcanic and plutonic rocks of Kotri belt and their coeval tectonic and magmatic episodes comparable with the emplacement age of Bijli rhyolite, Dongargarh and Malanjkhand granites.

- The geological, geochemical and geochronological (G^3) evidences suggest that island arc magmatism and subsequent crustal anatexis played a significant role for the evolution of Neoarchean-Paleoproterozoic crustal growth of Central Indian Cratons particularly within the time frame of 2.47-2.5 Ga.

Acknowledgements

The authors thank Dr. Ch Mohan Rao, Director, NGRI for permitting to publish this work. CM acknowledges the funds from Council of Scientific and Industrial Research (CSIR) to National Geophysical Research Institute through the projects of India Deep Earth Exploration Programme (INDEX) and MLP 6201-28 (CM). The authors gratefully acknowledge Prof. Sanghoon Kwon for editorial handling and two anonymous reviewers for their constructive comments and suggestions that helped to improve the standard of the manuscript. Dr. Kundan Banjara of Mines and Geology, Chhattisgarh is thanked for his help during the field work. Drs. M. Satyanarayanan, S. Sawanth, K.S.V. Subramanyam and A.K. Krishna are acknowledged for providing the geochemical data. Santosh is supported through Foreign Expert grants at the China University of Geosciences Beijing, China, and Professorial position at the University of Adelaide, Australia.

References

Ahmad, T., Wanjari, N., Kaulina, T.V., Mishra, M.K and Nitkina, E.A., (2008). Geochemical and isotopic characteristics of the Amgaon gneissic complex, Central Indian Shield: Constraints on Precambrian crustal evolution. In: Proc. Int. Symp. 'Geoscience Resources and Environments of Asian Terranes (GREAT-2008), 4th IGCP 516, and 5 APSEG;' Bangkok, Thailand.

Ahmad, T., Longjam, K.C., Fouzdar, B., Bickle, M.J., Chapman, H.J., 2009. Petrogenesis and tectonic setting of bimodal volcanism in the Sakoli Mobile belt, Central Indian Shield. Island Arc 18, 155-174.

Andersen, T., 2002. Correction of common lead in U-Pb analyses that do not report Pb-204. Chemical Geology 192, 59-79.

Arndt, N.T., Lesher, M., Barnes, S.-J., 2008. Komatiites. Cambridge University Press. Cambridge 467pp.

Arndt, N.T., Teixeira, N.A., White, W.M., 1989. Bizarre geochemistry of komatiites from the Crixas greenstone belt, Brazil. Contributions to Mineralogy and Petrology 101, 187-197.

Asthana, D., Khare, S.K., Pophare, A.M., Dash, M.R., 1997. Comment on "Geochemistry of Dongargarh volcanic rocks, Central India: implications for the Precambrian mantle". Precambrian Research 84, 105-107.

Asthana, D., Pophare, A.M., Rajalingam, S., Kumar, H., 2014. Neoarchaean Dongargarh Rapakivi A-type Granites and its relationship to Pitepani tholeiites. Gondwana Geological Magazine, Special Volume 16, 25-40.

Ayalew, D., Ishiwatari, A., 2011. Comparison of rhyolites from continental rift, continental arc and oceanic island arc: Implication for the mechanism of silicic magma generation. Island Arc 20, 78-93.

Barbarin, B., 2005. Mafic magmatic enclaves and mafic rocks associated with some granitoids of the central Sierra Nevada batholith, California: Nature, origin, and relations with the hosts. Lithos 80, 155-77.

Best, M.G., Christiansen, E.H., 2001. Igneous Petrology. Blackwell Science, Inc, 458 pp.

Black, L.P., Kamo, S.L., Allen, C.M., Davis, D.W., Aleinikoff, J.N., Valley, J.W., Mundil, R., Campbell, I.H., Korsch, R.J., Williams, I.S., 2004. Improved $^{206}Pb/^{238}U$ microprobe geochronology by the monitoring of a trace-element related matrix effect; SHRIMP, ID–TIMS, ELA–ICP–MS and oxygen isotope documentation for a series of zircon standards. Chemical Geology 205, 115–140.

Blichert-Toft, J., Albarède, F., 1997. The Lu–Hf geochemistry of chondrites and the evolution of the mantle–crust system. Earth and Planetary Science Letters 148, 243–258.

Bonev, N., Stampfli, G., 2008. Petrology, geochemistry and geodynamic implications of Jurassic island arc magmatism as revealed by mafic volcanic rocks in the Mesozoic low grade sequence, eastern Rhodope, Bulgaria. Lithos 100, 210-233.

Bonin, B., 2004. Do coeval mafic and felsic magmas in post-collisional to within-plate regimes necessarily imply two contrasting, mantle and crustal, sources? A review. Lithos 78, 1-24.

Bonin, B., 2007. A-type granites and related rocks: Evolution of a concept, problems and prospects. Lithos 97, 1-29.

Bonnefoi, C.C., Provost, A., Albarède, F., 1995. The 'Daly gap' as a magmatic catastrophe. Nature 378, 270-272.

Chu, N.C., Taylor, R.N., Chavagnac, V., Nesbitt, R.W., Boela, R.M., Milton, J.A., Germain,C.R., Bayon, G., Burton, K., 2002. Hf isotope ratio an analysis using multi-

collector inductively coupled plasma mass spectrometry: an evaluation of isobaric interference corrections. Journal of Analytical Atomic Spectrometry 17, 1567–1574.

Collins, W.J., Beams, S.D., White, A.J.R., Chappell, B.W., 1982. Nature and origin of A-type granites with particular reference to southeastern Australia. Contributions to Mineralogy and Petrology 80, 189-200.

Coward, M.P., Dewey, J.F., and Hancock, P.L., 1987. Continental extensional tectonics. Geological Society of London Special Publication 28, 1-637.

Cox, K.G., 1988. The Karoo Province, In: (Ed.) McDougal, J.D., Continental flood basalts. The Netherlands, Kluwer Academic, 279-321.

Creaser, R.A., Price, R.C., Wormald, R.J., 1991. A-type granites revisited: assessment of a residual source model. Geology 19, 163-166.

Dall'Agnol, R., Teixeira, N.P., Rämö, O.T., Moura, C.A.V., Macambira, M.J.B., Oliveira, D.C., 2005. Petrogenesis of the Paleoproterozoic, rapakivi, A-type granites of the Archean Carajás Metallogenic Province, Brazil. Lithos 80, 101-129.

Daly, R.A., 1925. The geology of Ascension Island. Proceeding of American Academy of Arts and Science 60, 1-80.

DeBievre, P., Taylor, P.D.P., 1993. Table of the isotopic composition of the elements. Journal of Mass Spectrometry. Ion Process, 123–149.

Deering, C.D., Cole, J.W., Vogel, T.A., 2008. A rhyolite compositional continuum governed by lower crustal source conditions in the Taupo volcanic zone, New Zealand. Journal of Petrology 49, 2245-2276.

Deering, C.D., Bachmann, O., Dufek, J., Gravley, D.M., 2011. Rift-Related transition from andesite to rhyolite volcanism in the Taupo Volcanic Zone (New Zealand) controlled by crystal-melt dynamics in mush zones with variable mineral assemblages. Journal of Petrology 52, 2243-2263.

Defant, M.J., Kepezhinskas, P., 2001. Evidence suggests slab melting in arc magmas. EOS 82, 65-69.

Dixon, S., Rutherford, M. J., 1979. Plagiogranites as late-stage immiscible liquids in ophiolite and mid-ocean ridge suites: an experimental study. Earth and Planetary Science Letters 45, 45-60.

Dobretsov, N.L., 2005. 250Ma large igneous provinces of Asia: Siberian and Emeishan traps (plateau basalts) and associated granitoids. Russian Geology and Geophysics 46, 847–868.

Duncan, A.R., Erlank, A.J., Marsh, J., 1984. Regional geochemistry of the Karoo igneous province. Special Publication Geological Society of Africa 13, 355-388.

Eby, G.N., 1992. Chemical subdivision of the A-type granitoids, petrogenetic and tectonic implications. Geology 20, 641-644.

Ellam, R.M., Hawkesworth,C.J., 1988.Elementaland isotopic variations in subductionrelated basalts: evidence for a three componentmodel. Contributions to Mineralogy and Petrology 98, 72-80.

Elliott, T., Plank, T., Zindler, A., 1997. Element transport from slab to volcanic front at the Mariana arc. Journal of Geophysical Research 102, 14991-15019.

Ewart, A., Collerson, K.D., Regelous, M., Wendt, J.I., Niu, Y., 1998. Geochemical evolution within the Tonga–Kermadec–Lauarc–back-arc systems; the role of varying mantle wedge composition in space and time. Journal of Petrology 39, 331-368.

Eyal, M., Litvinovsky, B., Jahn, B.M., Zanvilevich, A., Katzir, Y., 2010. Origin and evolution of postcollisional magmatism: Coeval Neoproterozoic calc-alkaline and alkaline suites of the Sinai Peninsula. Chemical Geology 269, 153–179.

Förster, H.J., Tischendorf, G., Trumbull, R.B., 1997. An evaluation of the Rb vs, (Y + Nb) discrimination diagram to infer tectonic setting of silicic igneous rocks. Lithos 40, 261-293.

Frei, R., Rosing, M., Waight, T.E., Krogstad, E.J., Storey, M., Ulfbeck, D.G., Albarède, F., 2002. Hydrothermal-metasomatic and tectonothermal processes in the Isua greenstone belt (West Greenland): a multi-isotopic investigation of their effects on the Earth's oldest oceanic crustal sequence. Geochimica et Cosmochimica Acta 66, 467–486.

Fretzdorff, S., Livermore, R.A., Devey, C.W., Leat, P.T., Stoffers, P., 2002. Petrogenesis of the back-arc east scotia ridge, south Atlantic ocean. Journal of Petrology 43, 1435-1467.

Freundt-Malecha, B., Schmincke, H.U., 2001. Plutonic rocks of intermediate composition on Gran Canaria: The missing link of the bimodal volcanic rock suite. Contributions to Mineralogy and Petrology 141, 430–445.

Frey, F.A., Gerlach, D.C., Hickey, R.L., Escobar, L.L., Villavicencio, F.M., 1984. Petrogenesis of the Laguna el Maule volcanic complex, Chile (36^{o}S). Contributions to Mineralogy and Petrology 88, 133-149.

Frost, C.D., Frost, B.R., 1997. Reduced rapakivi-type granites: The tholeiite connection. Geology 25, 647–650.

Frost, C.D., Frost, B.R., Chamberlain, K.R., and Edwards, B.E., 1999. Petrogenesis of the 1.43 Ga Sherman batholith, SE Wyoming, USA: A reduced, rapakivi-type anorogenic granite. Journal of Petrology 40, 1771-1802.

Gamble, J.A., Wright, I.C., Woodhead, J.D., Smith, I., 1995. Arc and back-arc geochemistry in the southern Kermadec arc–Ngatoro Basin and offshore Taupo Volcanic Zone, SW Pacific. In: Smellie, J.L. (Ed.), Volcanism Associated with Extension at Consuming Plate Margins. Geological Society of Special Publication, London, 193–212.

Garland, F., Hawkesworth, C.J., Mantovanim, S.M., 1995. Description and petrogenesis of the Parana rhyolites, southern Brazil. Journal of Petrology 36, 1193–1227.

Garland, F., Hawkesworth, C.J., Mantovani, M.S.M., 1997. Reply to the comment by Harris and Milner on the paper 'description and petrogenesis of the Paraná rhyolites, southern Brazil' by Garland et al. (1995). Journal of Petrology 38, 299-302.

Geist, D., Howard, K.A., Larson, P., 1995. The generation of oceanic rhyolites by crys-tal fractionation: the basalt–rhyolite association at Volcán Alcedo, Galápagos Archipelago. Journal of Petrology 36, 965-982.

Geng, J.Z., Li, H.K., Zhang, J.Q., Zhou, H.Y., Li, H.M., 2011. Zircon Hf isotope analysis by means of LA-MC-ICP-MS. Geological Bulletin of China 30, 1508-1513.

Geological Survey of India, 2004. Geology and Mineral map-District Resource Map, Rajnandagaon District, Chhattisgarh, First Edition, Kolkata.

Ghosh, J.G., 2004. 3.56 Ga tonalite in the central part of the Bastar Craton, India: oldest Indian date. Journal of Asian Earth Sciences 23, 359–364.

Ghosh, J.G., Pillay, K.R., 2012. Evolution of the Kotri Linear Belt: A Late Archaean Continental Rift in the Bastar Craton, Central India. Proceedings of the National workshop on "Recent advances in Geology of Dongargarh-Kotri belt, Central India and its Mineral potential". Gondwana Geological Society, Nagpur, p. 16.

Gilder, S.A., Keller, G.R., Luo, M., Goodell, P.C., 1991. Timing and spatial-distribution of rifting in China. Tectonophysics 197, 225-243.

Griffin, W.L., Pearson, N.J., Belousova, E., Jackson, S.E., van Achterbergh, E., O'Reilly, S.Y., Shee, S.R., 2000. The Hf isotope composition of cratonic man-tle: LA-MC-ICPMS analysis of zircon megacrysts in kimberlites. Geochimica et Cosmochimica Acta 64, 133–147.

Griffin, W.L., Wang, X., Jackson, S.E., Pearson, N.J., O'Reilly, S.Y., Xu, X., Zhou, X.,

2002. Zircon chemistry and magma mixing, SE China: in-situ analysis of Hf isotopes.Tonglu and Pingtan igneous complexes. Lithos 61, 237–269.

Hawkesworth, C.J., Hergt, J.M., Ellam, R.M., McDermott, F., 1991. Element fluxes associated with subduction related magmatism. Philosophical Transaction of Royal Society of London, A-335, 393-405.

Hochstaedter, A.G., Gill, J.B., Kusakabe, M., Newman, S., Prinle, M., Taylor, B., Fryer, P., 1990. Volcanism in the Sumisu Rift I: element, volatile and stable geochemistry. Earth Planetary Science Letters 100, 179-194.

Hollings, P., Wyman, D Kerrich, R., 1999. Komatiite-basalt-rhyolite volcanic associations in northern Superior Province greenstone belts: significance of plume-arc interaction in the generation of proto continental Superior Province. Lithos 46, 137-161.

Hupert, H.E., Sparks, R.S.J., 1985. Cooling and contamination of mafic and ultramafic magma during ascent through continental crust. Earth and Planetary Science Letters 74, 371ring.

Ikeda, Y., Yuasa, M., 1989. Volcanism in nascent backarc basins behind the Schichito Ridge and adjacent areas in the Izu-Ogasawara arc, NW Pacific; evidence for mixing between E-type MORB and island arc magmas at the initiation of backarc rifing. Contributions to Mineralogy and Petrology 101, 377-393.

Jahn, B.M., Litvinovsky, B.A., Zanvilevich, A.N., Reichow, M., 2009. Peralkaline granitoid magmatism in the Mongolian–Transbaikalian belt: Evolution, petrogenesis and tectonic significance. Lithos 113, 521-539.

Jochum, K.P., Arndt, N.T., Hoffman, A.W., 1991. Nb–Th–La in komatiites and basalts: constraints on komatiites petrogenesis and mantle evolution. Earth and Planetary Science Letters 107, 272–289.

Jordan, B.T., Grunder, A.L., Duncan, R.A., Deino, A.L., 2004. Geochronology of age-progressive volcanism of the Oregon High Lava Plains: implications for the plume interpretation of Yellowstone. Journal of Geophysical Research-Solid Earth 109, B10202.

Jung, C., Jung, S., Hoffer, E., Berndt, J., 2006. Petrogenesis of Tertiary mafic alkaline magmas in the Hocheifel, Germany. Journal of Petrology 47, 1637–1671.

Kepezhinskas, P., Defant, M.J., Drummond, M.S., 1996. Progressive enrichment of island arc mantle by melt periodotite interaction inferred from Kamchatcka xenoliths. Geochimica et Cosmochimica Acta 60, 1217-1229.

Krishnamurthy, P., Sinha, D.K., Rai, A.K., Seth, D.K., Singh, S.N., 1990. Magmatic rocks of the Dongargarh Supergroup, central India-their petrological evolution and implications on metallogeny. Geological Survey of India Special Publication 28, 309-319.

Lafleche, M.R., Dupuy, C., Dostal, J., 1992. Tholeiitic volcanic rocks of the late Archaean Blake River group, southern Abitibi greenstone belt: origin and geo-dynamic implications. Canadian Journal of Earth Science 29, 1448–1458.

Langmuir C. H., Vocke J. R. R. D., Hanson G. N., Hart S. R., 1978. A general mixing equation with application to Icelandic basalts. Earth and Planetary Science Letters 37, 380-92.

Le Bas, M. J., Le Maitre, R.W., Streckeisen, A., Zanettin, B., 1986. A chemical classification of volcanic rocks based on the total alkali-silica diagram. Journal of Petrology 27, 745-750.

le Roux, P.J., le Roex, A.P., Schilling, J.G., Schmizu, N., Perkins, W.W., Pearce, N.J.G., 2002. Mantle heterogeneity beneath the southern Mid-Atlantic ridge: Trace element evidence for contamination of ambient asthenospheric mantle. Earth and Planetary Science Letters 203, 479-498.

Lesher, C.M., Arndt, N.T., 1995. REE and Nd isotope geochemistry, petrogenesis and volcanic evolution of contaminated komatiites at Kambalda, Western Australia. Lithos 34, 127-157.

Lesher, C.M., Goodwin, A.M., Campbell, I.H., Gorton, M.P., 1986. Trace element geochemistry of ore associated and barren felsic metavolcanic rocks in the Superior Province, Canada. Canadian Journal of Earth Sciences 23, 222-237.

Lesher, C.E., Cashman, K.V., Mayfield, J.D., 1999. Kinetic controls on crystallization of Tertiary North Atlantic basalt and implications for the emplacement and cooling history of lava at site 989, southeast Greenland rifted margin. Proceedings of Ocean Drilling Programme Scientific Research 161, 135llto.

Lesher, C.M., Burnham, O.M., Keays, R.R., 2001. Trace element geochemistry and petrogenesis of barren and ore association komatiites. Canadian Mineralogies 39, 673-696.

Li, X.H., Li, Z.X., Zhou, H., Liu, Y., Kinny, P.D., 2002. U–Pb zircon geochronology, geochemistry and Nd isotopic study of Neoproterozoic bimodal volcanic rocks in the Kangdian Rift of South China: implications for the initial rifting of Rodinia. Precambrian Research 113, 135–154.

Li, Z.X., Li, X.H., Kinny, P.D., Wang, J., Zhang, S., Zhou, H., 2003. Geochronology of Neoproterozoic syn-rift magmatism in the Yangtze Craton, South China and correlations with other continents: evidence for a mantle superplume that broke up Rodinia. Precambrian Research 122, 85–109.

Li, W.X., Li, X.H., Li, Z.X., 2005. Neoproterozoic bimodal magmatism in the Cathaysia Block of South China and its tectonic significance. Precambrian Research 136, 51–66.

Li, H.K., Geng, J.Z., Zheng, S., Zhang, Y.Q., Li, H.M., 2009. Zircon U-Pb age dating by means of LA-ICP-MS. Acta Mineralogica Sinica, 600-601.

Litvinovsky, B.A., Jahn, B., Zanvilevich, A.N., Saunders, A., Poulain, S., Kuzmin, D.V., Reichow, M.K., Titov, A.V., 2002. Petrogenesis of syenite–granite suites from the Bryansky Complex (Transbaikalia, Russia): Implications for the origin of A-type granitoid magmas. Chemical Geology 189, 105-133.

Ludden, J., Gelienas, L., Trudel, P., 1982. Archaean metavolcanics from the Rouyn-Noranda District, Abitibi greenstone belt, Quebec: 2 mobility of trace elementsand petrogenetic constraints. Canadian Journal of Earth Science 19, 2276–2287.

Ludwig, K.R., 2003. ISOPLOT 3.0: A Geochronological Toolkit for Microsoft Excel. Berkeley Geochronology Center. Special, Publication No. 4.

Manikyamba, C., Kerrich, R., Khanna, T. C., Krishna, A. K., Satyanarayanan, M., 2008. Geochemical systematics of komatiite-tholeiite and adakite-arc basalt associations: the role of a mantle plume and convergent margin in formation of the Sandur Superterrane, Dharwar Craton. Lithos 106, 155-172.

Manikyamba, C., Saha, A., Ganguly, S., Santosh, M., Lingadevaru, M., Singh, M.R., Subba Rao, D.V. 2014a. Sediment-infill volcanic breccias from the Neoarchean Shimoga greenstone terrane, western Dharwar Craton: implications on pyroclastic volcanism and sedimentation in an active continental margin. Journal of Asian Earth Sciences 96, 269-278.

Manikyamba, C., Saha, A., Santosh, M., Ganguly, S., Singh, M.R., Subba Rao, D.V.,2014b. Neoarchean felsic volcanic rocks from the Shimoga greenstone belt,Dharwar Craton, India: geochemical fingerprints of crustal growth at an active continental margin. Precambrian Research 252, 1–21

Manikyamba C., Ganguly S., Santosh M., Saha A., Chatterjee A., Khelen A.C. 2015. Neoarchean arc-juvenile back-arc magmatism in eastern Dharwar Craton, India: geochemical fingerprints from the basalts of Kadiri greenstone belt. Precambrian Research, 258, 1-23.

Marlina, A.E., John, F., 1999. Geochemical response to varying tectonic settings: an example from southern Sulawesi (Indonesia). Geochimica et Cosmochimica Acta 63, 1155-1172.

Meade, F.C., Troll, V.R., Ellam, R.M., Freda, C., Font, L., Donaldson, C.H., Klonowska, I., 2014. Bimodal magmatism produced by progressively inhibited crustal assimilation. Nature doi:10.1038/ncomms5199Mishra, V.P., Singh, P., Dutta, N.K., 1988. Stratigraphy, structure and metamorphic history of Bastar district, Madhya Pradesh Records of Geological Survey of India 117, 1-26.

Moraes, R., Fuck, R.A., Pimentel, M.M., Gioia, S.M.C.L., Figueiredo, A.M.G., 2003.Geochemistry and Sm-Nd isotopic characteristics of bimodal volcanic rocks of Juscelandia, Goias, Brazil: Mesoproterozoic transition from continental rift to ocean basin. Precambrian Research 125, 317-336.

Morata, D., Aguirre, L., Oyarzún, M., Vergara, M., 2000. Crustal contribution in the genesis of the bimodal Triassic volcanism from the Coastal Range, central Chile. Revista Geológica de Chile 1, 27.

Mukhopadhyay, J., Beukes, N.J., Armstrong, R.A., 2012. Depositional Setting and New Age Constraints of the Bailadila Group, Bastar Craton: Implications for the Oldest 'Superior Type' Iron Formation in India and its Economic Potential. Proceedings of the National workshop on “Recent advances in Geology of Dongargarh-Kotri belt, Central India and its Mineral potential”. Gondwana Geological Society, Nagpur, p. 22-23.

Munker, C., Womer, G., Yogodzinski, G., Churikova, T. 2004. Behavior of high field strength element elements in subduction zones constraints from Kamchatka-Aleutian arc lavas. Earth and Planetary Science Letters 224, 275-293.

Mushkin, A., Navon, O., Halicz, L., Hartmann, G., Stein, M., 2003. The petrogenesis of A-type magmas from the Amram Massif, southern Israel. Journal of Petrology 44, 815-832.

Naqvi, S.M., Rogers, J.J.W., 1987. Precambrian Geology of India. Oxford University Press, New York, pp. 223.

Neogi, S., Miura, H., Hariya, Y., 1996. Geochemistry of Dongargarh volcanic rocks, central India: implications for the Precambrian mantle. Precambrian Research 76, 77–91.

Nono, A., DeÂruelle, B., Demaiffe, D., Kambou, R., 1994. Tchabal Nganha volcano in Adamawa (Cameroon): Petrology of a continental alkaline lava series. Journal of Volcanology and Geothermal Research 60, 147-178.

Panigrahi, M.K., Misra, K.C., Brteam, B., Naik, R.K., 2002. Genesis of the granitoid copper–molybdenum mineralization at Malanjkhand, central India: facts and problems (extended abs.). Proceedings of the 11th Quadrennial International Associations on the Genesis of Ore Deposits Symposium and Geocongress, Windhock, Namibia.

Pearce, J.A., 2008. Geochemical fingerprinting of oceanic basalts with applications to ophiolite classification and the search for Archean oceanic crust. Lithos 100, 14–48.

Pearce, J.A., 1982. Trace element characteristics of lavas from destructive plate boundaries. John Wiley and Sons, United Kingdom (GBR), Chichester, pp. 525-548.

Pearce, J.A., Peate, D.W., 1995. Tectonic implications of the composition of volcanic arc magmas. Annual Reviews of Earth and Planetary Sciences 23, 251-285.

Pearce, J.A., Baker, P.E., Harvey, P.K., Luff, I.W., 1995. Geochemical evidence for subduction fluxes, mantle melting and fractional crystallization beneath the South Sandwich island arc. Journal of Petrology 36, 1073-1109.

Pearce, J.A., Kempton, P.D., Nowell, G.M., Noble, S.R., 1999. Hf–Nd element an isotope perspective on the nature and provenance of mantle and subduction components in Western Pacific arc-basin systems. Journal of Petrology 40, 1579-1611.

Peccerillo, A., Barberio, M.R., Yirgu, G., Ayalew, D., Barbieri, M., Wu, T.W., 2003. Relationship between mafic and peralkaline felsic magmatism in continental rift settings: A petrological, geochemical and isotopic study of the Gedemsa Volcano, Central Ethiopian Rift. Journal of Petrology 44, 2003-2032.

Peccerillo, A., Barberio, M.R., Yirgu, G., Ayalew, D., Barbieri, M., Wu, T.W., 2003. Relationship between mafic and peralkaline felsic magmatism in continental rift settings: A petrological, geochemical and isotopic study of the Gedemsa Volcano, Central Ethiopian Rift. Journal of Petrology 44, 2003-2032.

Pe-Piper G, Moulton B., 2008. Magma evolution in the Pliocene-Pleistocene succession of Kos, South Aegean arc (Greece). Lithos 106, 110-124.

Petrone, C.M., Ferrari, L., 2008. Quaternary adakite – Nb enriched basalt association in the western Trans-Mexican Volcanic Belt: Is there any slab melt evidence? Contributions to Mineralogy and Petrology 156, 73-86.

Pin, C., Paquette, J.L., 1997. A mantle-derived bimodal suite in the Hercynian belt: Nd isotope and trace element evidence for a subduction-related rift origin of the Late Devonian Brevenne metavolcanics, Massif Central (France). Contributions to Mineralogy and Petrology 129, 222–238.

Pin, C., Marini, F., 1993. Early Ordovician continental break-up on Variscan Europe: Nd–Sr isotope and trace element evidence for bimodal igneous associations of the southern Massif Central, France. Lithos 29, 177-196.

Polat, A., Hofmann, A.W. 2003. Alteration and geochemical patterns in the 3.7–3.8 Ga Isua greenstone belt, West Greenland. Precambrian Research 126, 197-218.

Polat, A., Hofmann, A.W., Rosing, M.T., 2002. Boninite-like volcanic rocks in the 3.7–3.8 Ga Isua greenstone belt, West Greenland: geochemical evidence for intra-oceanic subduction zone processes in the early Earth. Chemical Geology 184, 231–254.

Rai, A.K., Sinha, D.K., Parihar, P.S., 2012. A Geochemical Approach towards the Tectonic Environment of Basic Meta-volcanics (Pitepani Volcanics) of Bodal Bhandaritola area Rajnandgaon District, Chhattisgarh. Proceedings of the National workshop on "Recent advances in Geology of Dongargarh-Kotri belt, Central India and its Mineral potential". Gondwana Geological Society, Nagpur, pp.24.

Rajesh, H.M., Mukhopadhyay. J, Beukes. N.J., Belyanini, G.A., Armstrong, R.A., 2009. Evidence for an early Archaean granite from Bastar craton, India. Journal of Geological Society of London 166, 193–196.

Ramachandra, H.M., Roy, A., 1998. Geology of intrusive granitoids with particular reference to Dongargarh granite and their impact on tectonic evolution of the Precambrian in Central India. Indian Minerals 52, 15-32.

Ramachandra, H.M., Roy, A., Mishra, V.P., Dutta, N.K., 2001. A critical review of the tectonothermal evolution of the Bastar craton. Geological Survey of India Special Publication 55, 161-180.

Ramachandra, H.M., Roy, A., 2012. A review of evolutionary characteristics of the Bastar Craton. Proceedings of the National workshop on "Recent advances in Geology of

Dongargarh-Kotri belt, Central India and its Mineral potential". Gondwana Geological Society, Nagpur, p. 3-7.

Ramakrishnan, M., Vaidyanathan, R., 2008. Geology of India. Vol 1, Geological Society of India, 556 pp.

Ramakrishnan, M., 1990. Crustal development in Southern Bastar, Central Indian craton. Geological Survey of India Special Publication 28, 44-66.

Rämö, O.T., Haapala, I., Vaasjoki, M., Yu, J.H., Fu, H.Q., 1995. 1700 Ma Sachang complex, northeast China: Proterozoic rapakivi granite not associated with Paleoproterozoic orogenic crust. Geology 23, 815-818.

Ren, J.Y., Tamaki, K., Li, S.T., Zhang, J.X., 2002. Late Mesozoic and Cenozoic rifting and its dynamic setting in Eastern China and adjacent areas. Tectonophysics 344, 175-205.

Rollinson, H.R., 1993. Using geochemical data: Evaluation, presentation, interpretation. Harlow, Longman Scientific and Technical, pp. 352.

Rooney, T., Hart, W., Hall, C., Ayalew, D., Ghiorso, M., Hidalgo, P., Yirgu, G., 2012. Peralkaline magma evolution and the tephra record in the Ethiopian Rift. Contributions to Mineralogy and Petrology 164, 407-426.

Roy, A., Hanuma Prasad, M., Bhowmik, S.K., 2001. Recognition of Pre-Grenvillian and Grenvillian Tectonothermal Events in the Central Indian Tectonic Zones: Implications on Rodinian Crustal Assembly. Gondwana Research 4, 755-757.

Roy, A., Hanuma Prasad, M., 2003. Tectonothermal events in Central Indian Tectonic Zone (CITZ) and its implications in Rodinian crustal assembly. Journal of Asian Earth Sciences 22, 115-129.

Roy, A., Ramachandra, H.M., 2012. Emplacement of Neoarchean-Paleoproterozoic granitoids in Dongargarh-Kotri cratonic rift zone: implications for crustal growth and evolution of Bastar Cratob in Central India. Proceedings of the National workshop on

"Recent advances in Geology of Dongargarh-Kotri belt, Central India and its Mineral potential". Gondwana Geological Society, Nagpur, p. 8-11.

Rudnick, R.L., 1990. Continental crust: Growing from below. Nature 347, 711-2

Ryerson, F. J., Hess, P. C., 1978. Implications of liquid-liquid distribution coefficients to mineral-liquid partitioning. Geochimica et Cosmochimica Acta 42, 921-32.

Said, N., Kerrich, R., 2009. Geochemistry of coexisting depleted and enriched Paringa Basalts, in the 2.7 Ga Kalgoorlie Terrane, Yilgarn Craton, Western Australia: Evidence for a heterogeneous mantle plume event. Precambrian Research 174, 287-309.

Said, N., Kerrich, R., Maier, W.D., McCuaig, C., 2011. Behaviour of Ni–PGE–Au–Cu in mafic–ultramafic volcanic suites of the 2.7 Ga Kambalda Sequence, Kalgoorlie Terrane, Yilgarn Craton. Geochimica et Cosmochimica Acta 75, 2882-2910.

Sajona, F.G., Maury, R.C., Bellon, H., Cotton, J., Defant, M., 1996. High field strength element enrichment of Pliocene-Pleistocene island arc basalts, Zamboanga Peninsula, Western Mindanao Philippines. Journal of Petrology 37, 693-26.

Sarkar, S.N., Sarkar, S.S., Ray, S.L., 1994. Geochemistry and genesis of the Dongargarh Supergroup Precambrian rocks in Bhandara-Durg Region, central India. Indian Journal of Earth Sciences 21, 117–126.

Saunders, A.D., Norry, M.J., Tarney, J., 1991. Fluid influence on the trace element compositions of subduction zone magmas. Philosophical Transaction of Royal Society of London, A-335,377-392.

Scherer, E., Munker, C., Mezger, K., 2001. Calibration of the lutetium–hafnium clock. Science 293, 683–687.

Schiano, P., Clocchiatti, R., Shimizu, N., Maury, R.C., Jochum, K.P., Hofmann, A.W., 1995. Hydrous, silica-rich melts in the sub-arc mantle and their relationship with the erupted arc lavas. Nature 377, 595-600.

Sensarma, S., Palme, H., 2013. Silicate liquid immiscibility in the ~ 2.5 Ga Fe-rich andesite at the top of the Dongargarh large igneous province (India). Lithos 170-171, 239-251.

Shandl, E.S., Gorton, M.P., 2002. Applications of high field strength elements to discriminate tectonic settings in VMS environments. Economic Geology 97, 629-642.

Sharma, R.S., 2009. Cratons and Fold Belts of India. Springer Verlag, Heidelberg, pp.324.

Shinjo, R., Kato, Y., 2000. Geochemical constraints on the origin of bimodal magmatism at the Okinawa Trough, an incipient back-arc basin. Lithos 54, 117-137.

Shivkumar, K., Jain, P. K., Choudhary, D. K., Saxena, V. P., 2003. Geochemistry of Supracrustals of Kotri-Dongargarh Superagroup. Gondwana Geological Magazine Special volume 7, 217-239.

Shivkumar, K., Choudhary, D.K., Jain, P.K., Ramesh Babu, P.V., 2012. Geochemistry of bimodal volcanics and associated granitoids of Kotri-Dongargarh belt: an evidence for rift tectonics in Bastar Craton. Proceedings of the National workshop on "Recent advances in Geology of Dongargarh-Kotri belt, Central India and its Mineral potential". Gondwana Geological Society, Nagpur, pp. 25.

Song, X.Y., Zhou, M.F., Keays, R.R., Cao, Z.M., Sun, M., Qi, L., 2006. Geochemistry of the Emeishan flood basalts at Yangliuping, Sichuan, SW China: implications for sulphide segregation. Contributions to Mineralogy and Petrology 152 (1), 53-74.

Stein, H.J., Hannah, J.I.,Zimmerman, A., Markey, R.J., Sarkar, S.C., Pal, A.B., 2004. A 2.5 Ga porphyry Cu-Mo-Au deposit at Malanjkhand, Central India: implications for late Archean continental assembly. Precambrian Research 134, 189-226.

Sun, S.-S., Nesbitt, R.W., 1978. Geochemical regularities and genetic significance of ophiolitic basalts. Geology 6, 689–693.

Sun, S.S., Mc Donough, W.F., 1989. Chemical and isotopic systematics of oceanic basalts, implications for mantle composition and processes. In: Saunders, A.D., Norry, M.J.

(Eds.), Magmatism in the ocean basins. Geological Society of London Special Publication 42, Blackwell Scientific Publication, UK, pp. 313–345.

Tamura, Y., Tatsumi, Y., 2002. Remelting of an andesitic crustas a possible origin for rhyolitic magma in oceanic arcs: an example from the Izu-Bonin arc. Journal of Petrology 43,1029-1047.

Turner, S.P., Foden, J.D., Morrison, R.S., 1992. Derivation of some A-type magmas by fractionation of basaltic magma: an example from the Padthaway Ridge, South Australia. Lithos 28, 151-179.

Vernon, R. H., 1983. Restite, xenoliths and microgranitoid enclaves in granites. Journal and Proceedings of the Royal Society of New South Wales 116, 77-103.

Volpe, A.M., Macdougall, J.D., and Hawkins, J.W., 1987, Mariana Trough basalts (MTB): Trace element and Sr-Nd isotopic evidence for mixing between MORB-like and arc-like melts. Earth and Planetary Science Letters 82, 241-254.

Wang, Y., Qian, Q., Liu, L., Zhang, Q., 2000. Major geochemical characteristics of bimodal volcanic rocks in different geochemical environments. Acta Petrologica Sinica 16, 169-173.

Watson, E. B., 1979. Apatite- saturation in basic to intermediate magmas. Geophysical Research Letters 6, 937-40.

Wiedenbeck, M., Hanchar, J.M., Peck,W.H., Sylvester, P., Valley, J.,Whitehouse, M., Kronz, A., Morishita, Y., Nasdala, L., Fiebig, J., 2004. Further characterisation of the 91500 zircon crystal. Geostandards and Geoanalytical Research 28, 9–39.

Weinberg, R. F., 1997. The disruption of a diorite magma pool by intruding granite: The Sobu body, Ladakh batholith, Indian Himalayas. Journal of Geology 105, 87-98.

Whalen, J.B., Currie, K.L., Chappell, B.W., 1987. A-type granites, geochemical characteristics, discrimination and petrogenesis. Contributions to Mineralogy and Petrology 95, 407-419.

Whalen, J.B., Jenner, G.A., Longstaffe, F.J., Robert, F., Gariepy, C., 1996. Geochemical and isotopic (O, Nd, Pb and Sr) constraints on A-type granite petrogenesis based on the Topsails igneous suite, Newfoundland Appalachians. Journal of Petrology 37, 1463-1489.

Wilson, M., 1989, Igneous petrogenesis: London, Uniwin Hyman.

Woodhead, J.D., Eggins, S.M., Gamble, J.G., 1993. High field strength and transition element systematics in coupled arc-back arc settings: evidence for multi-phase melt extraction and a depleted mantle wedge. Earth Planetary Science Letters 114, 491-504.

Yamamoto, J., Kaneoka, I., Nakai, S., Kagi, H., Pridhod'ko, V.S., Arai, S., 2004. Evidence for subduction-related components in the subcontinental mantle from low $^{3}He/^{4}He$ and $^{40}Ar/^{36}Ar$ ratio in the mantle xenoliths from Far Eastern Russia. Chemical Geology 207, 237-259.

Yang, J.H., Sun, J.F., Chen, F.K., Wilde, S.A., Wu, F.Y., 2007. Sources and petrogenesis of Late Triassic dolerite dikes in the Liaoning Peninsula: Implications for post-collisional lithosphere thinning of the Eastern North China Craton. Journal of Petrology 48, 1973-1997.

Yuan, H.L., Gao, S., Liu, X.M., Li, H.M., Günther, D., Wu, F.Y., 2004. Accurate U–Pb age and trace element determinations of zircon by laser ablation-inductively coupled plasma-mass spectrometry. Geostandards and Geoanalytical Research 28, 353–370.

Yuan, H.L., Gao, S., Dai, M.N., Zong, C.L., Günther, D., Fontaine, G.H., Liu, X.M., Diwu, C.R., 2008. Simultaneous determinations of U–Pb age, Hf isotopes and trace element compositions of zircon by excimer laser-ablation quadrupole and multiple-collector ICP-MS. Chemical Geology 247, 100–118.

Zhang, X., Zhang, H., Tang, Y., Wilds, S.A., Hu, Z., 2008. Geochemistry of Permian bimodal volcanic rocks from central Inner Mangolia, North China: implications for tectonic setting and Phanerozoic continental growth in Central Asian Orogenic belt. Chemical Geology 249, 262-281.

Figure Captions

Fig. 1: Inset A) different cratons of India (after Sharma, 2009), B) geological map of Bastar Craton (after Naqvi and Rogers, 1987) and C) geological map of Kotri belt (after Geological Survey of India, 2004).

Fig. 2: Field photos of A) mafic volcanic rocks, B) felsic volcanic rock C) flow feature in rhyolite and D) outcrop of granite

Fig. 3: A) and B) Photomicrographs of mafic volcanic rocks showing intergranular and spherulitic textures; C) felsic rocks showing the presence of plagioclase, quartz and K-feldspar as phenocrysts floating within the siliceous groundmass; D) occurrence of primary flow texture in rhyolites; E) occurrence of plagioclase lamellae within microcline grain showing perthitic intergrowth in granite and F) presence of quartz intergrowth within potash feldspar depicting graphic texture.

Fig. 4: SiO_2 vs. major element oxides showing the bimodal nature of the analysed rocks.

Fig. 5: (A) Total alkali-silica classification diagram (Le Bas et al., 1986) in which the mafic and felsic rocks plot in the field of basalt and rhyolite.

Fig. 6: (A) and (C) are primitive mantle normalized multi-element diagram and B and D are chondrite normalized REE patterns of bimodal basalt-rhyolite association. Normalizing factors are from Sun and McDonough (1989).

Fig. 7: (A) Ab-An-Or ternary plot in which the analyzed samples plot in the field of granite; (B) Primitive mantle normalized multi-element diagram of granites; (C) Chondrite normalized REE of granites. Normalizing factors are from Sun and McDonough (1989).

Fig. 8: Cathodoluminescence (CL) images of representative zircons in the analysed samples from rhyolites (KB-26 and KB-35), basalt (KB-55) and granite (KB-127A). Yellow circles represent U-Pb age and red circles represent εHf (t) value.

Fig. 9: Zircon U–Pb concordia plots and age data histograms with probability curves for samples KB-55, KB-26, KB-35 and KB-127A from Nandagaon Group of Kotri belt, Bastar Craton, Central India.

Fig. 10: Hf(t) plots for zircons from the mafic, felsic rocks and granite of Kotri belt, Central India.

Fig. 11: A) Nb/Yb vs. Th/Yb diagram (after Pearce, 2008) in which Kotri mafic volcanic rocks plot above the NMORB-OIB array indicating a subduction component; (B) variation of La/Yb vs. Dy/Yb for the mafic volcanic rocks of Kotri belt reflecting on spinel-peridotite melting regime for the generation of basalts (after Jung et al., 2006) and (C) Th/Hf vs. Ta/Hf discrimination figure (after Shandl and Gorton, 2002) indicating active continental margin setting for the rhyolites of Kotri belt.

Fig. 12: (A) 10^4Ga/Al vs. Zr plot (Whalen et al., 1987) displaying A-type affinity of the granites (B) Y+Nb vs. Rb plot indicating within-plate type of analysed granites.

Fig. 13: Schematic diagram showing bimodal volcanism and granitoid emplacement in Kotri belt.

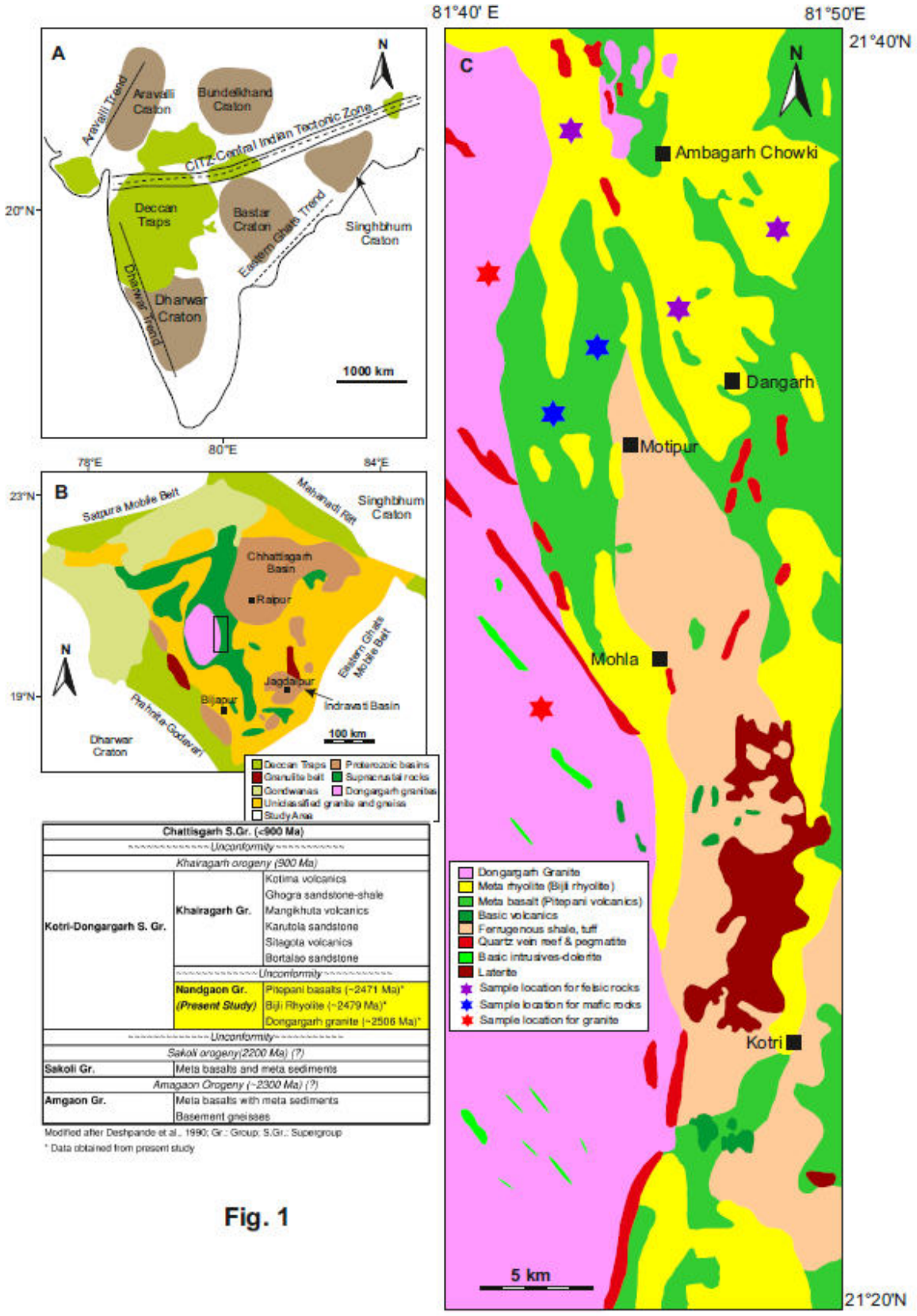

Chattisgarh S.Gr. (<900 Ma)		
~~ Unconformity ~~~~~~~~~~~~~~		
Khairagarh orogeny (900 Ma)		
Kotri-Dongargarh S. Gr.	Khairagarh Gr.	Kotima volcanics
		Ghogra sandstone-shale
		Mangikhuta volcanics
		Karutola sandstone
		Silagota volcanics
		Bortalao sandstone
	~~ Unconformity ~~~~~~~~~~~~~~	
	Nandgaon Gr. (Present Study)	Pitepani basalts (~2471 Ma)*
		Bijli Rhyolite (~2479 Ma)*
		Dongargarh granite (~2506 Ma)*
~~ Unconformity ~~~~~~~~~~~~~~		
Sakoli orogeny(2200 Ma) (?)		
Sakoli Gr.	Meta basalts and meta sediments	
Amgaon Orogeny (~2300 Ma) (?)		
Amgaon Gr.	Meta basalts with meta sediments	
	Basement gneisses	

Modified after Deshpande et al., 1990; Gr.: Group; S.Gr.: Supergroup

* Data obtained from present study

Fig. 1

Fig. 2

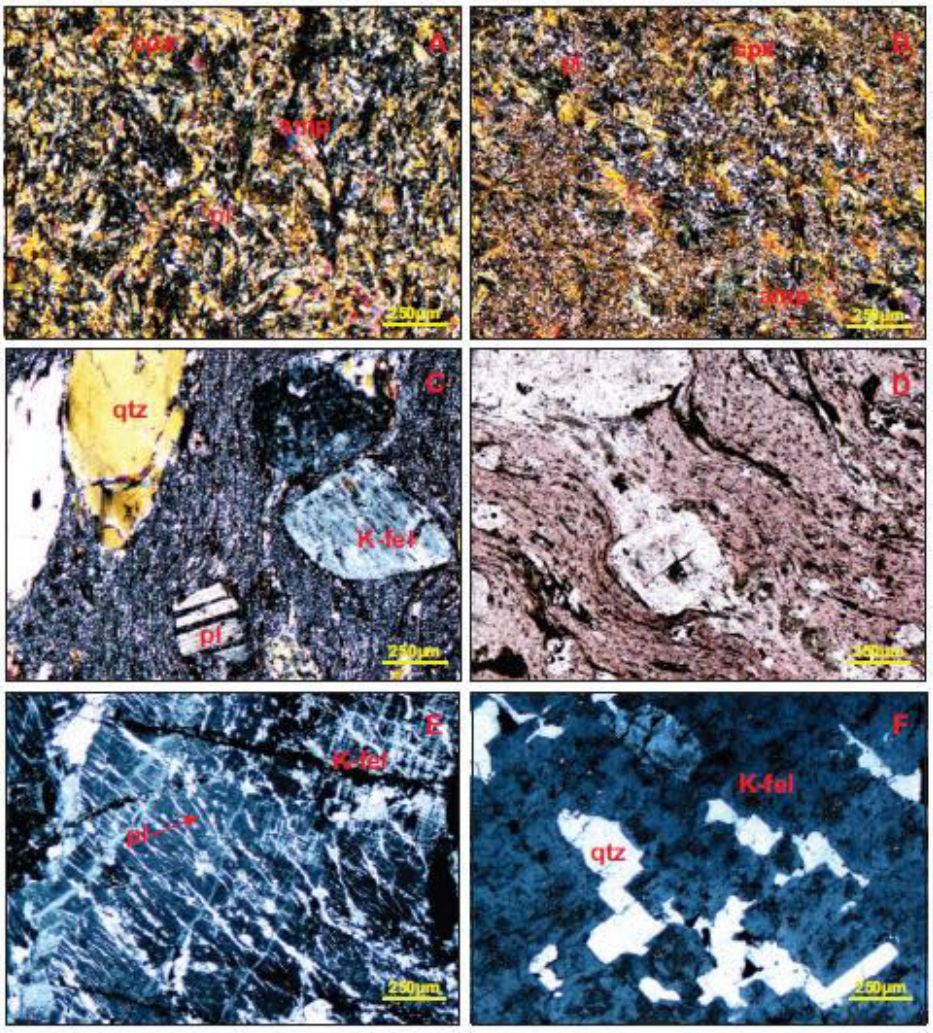

Fig.3

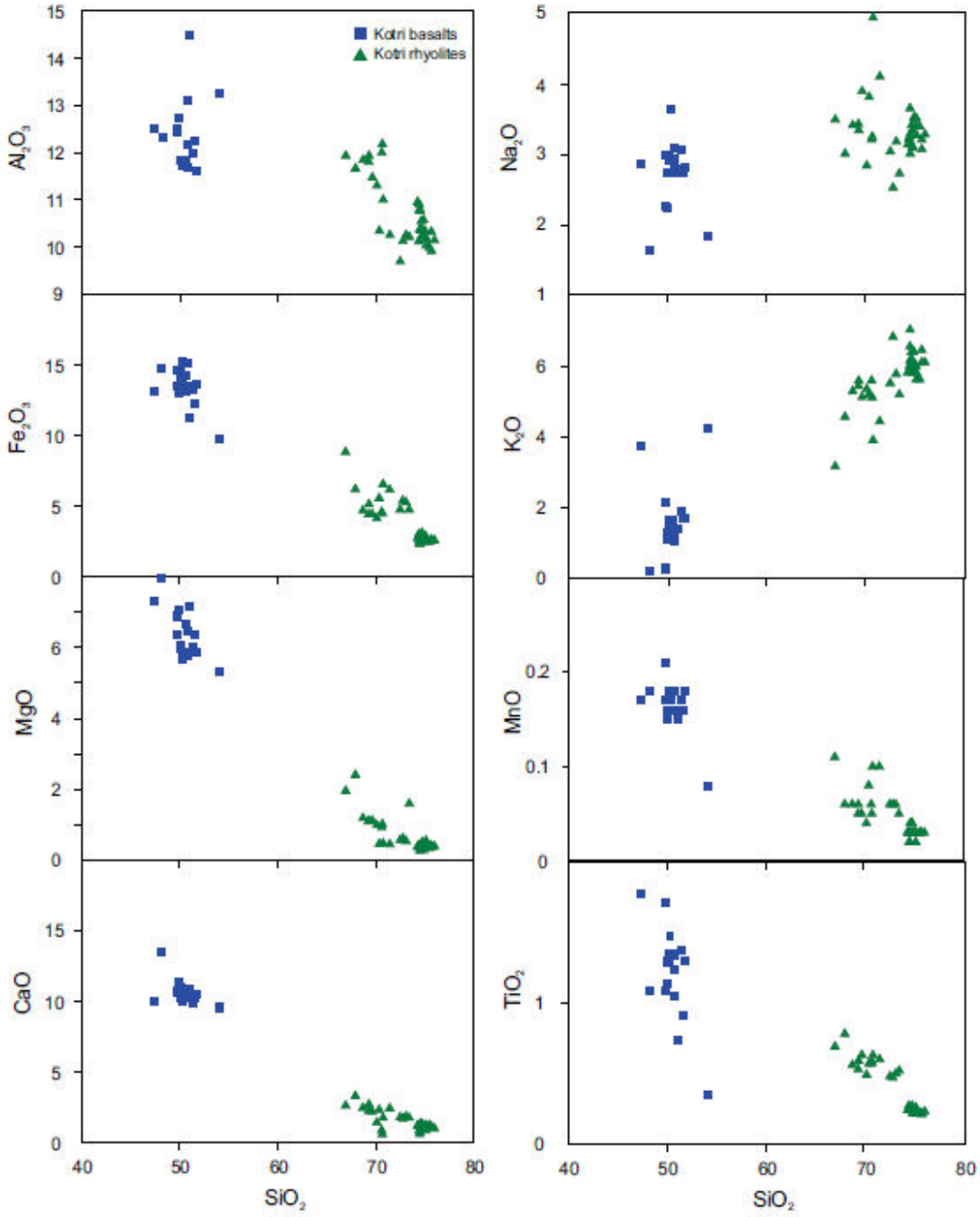

Fig. 4

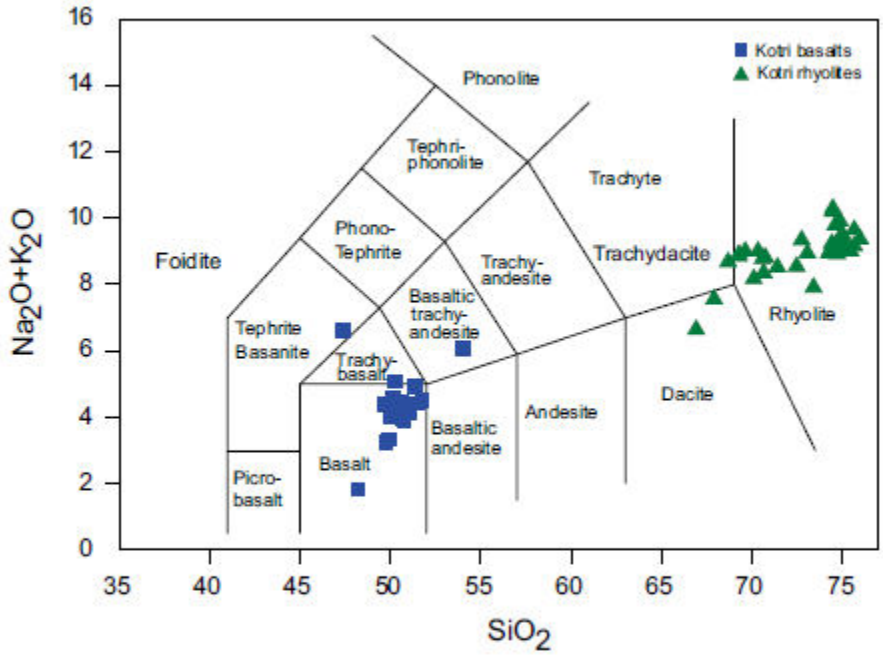

Fig. 5

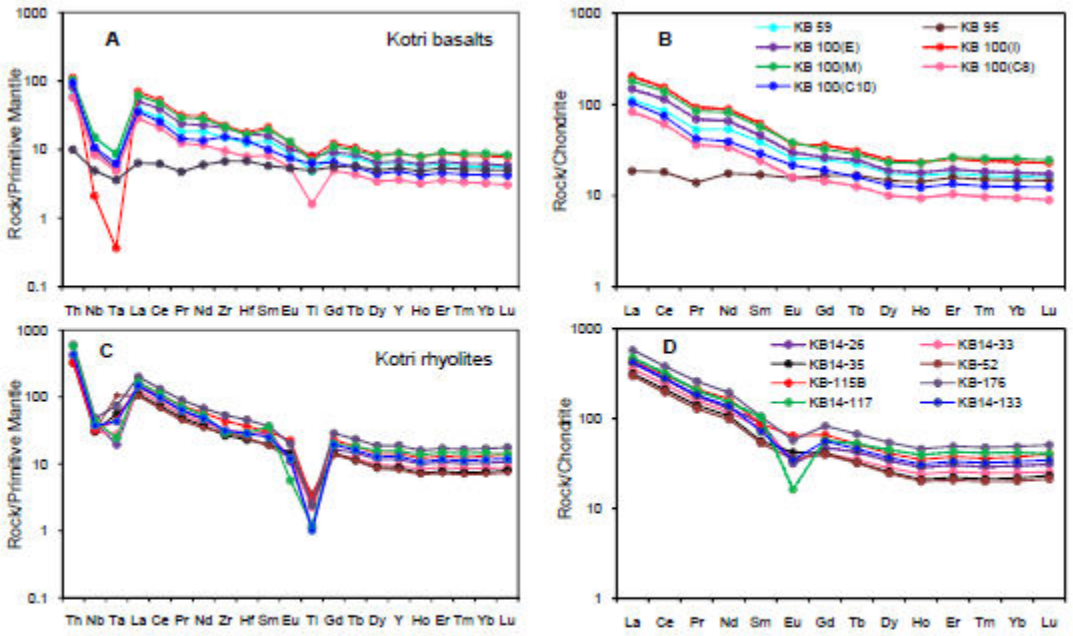

Fig.6

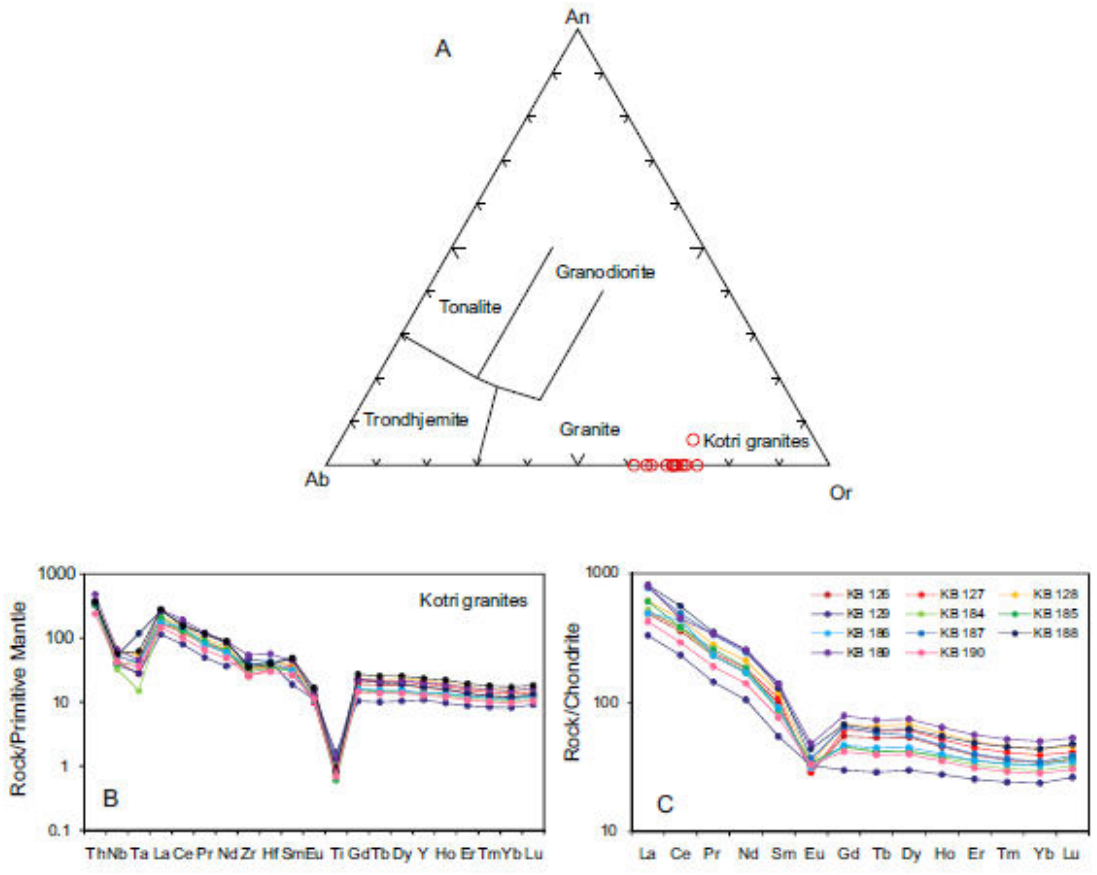

Fig.7

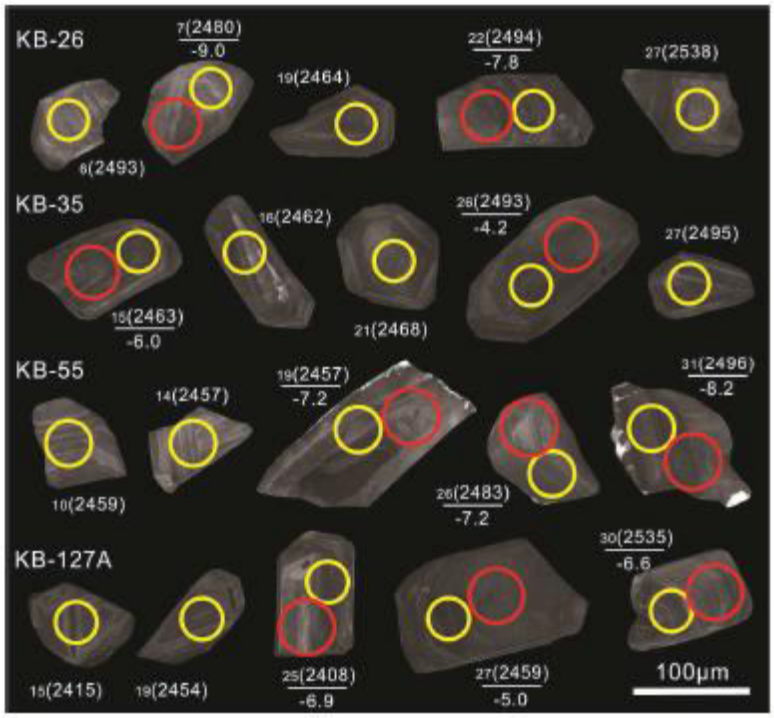

Fig. 8

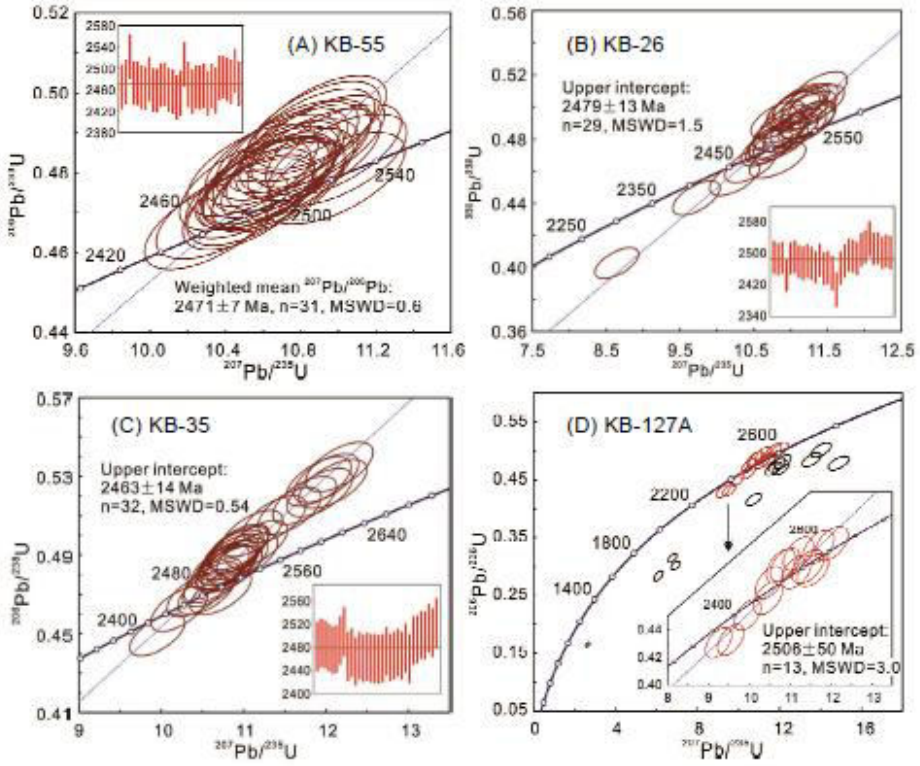

Fig. 9

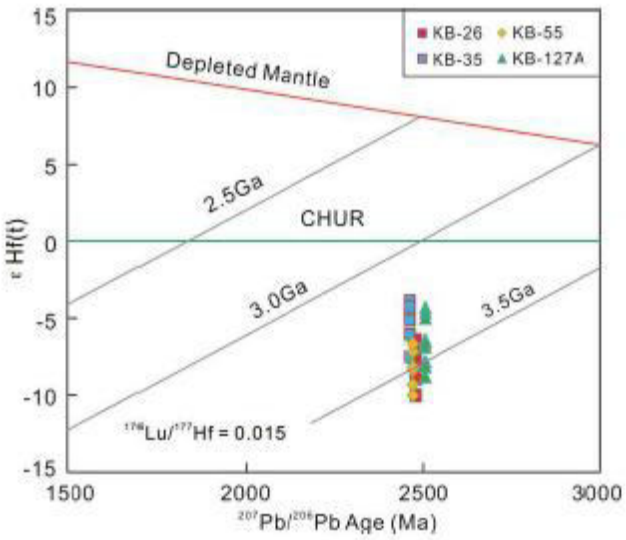

Fig. 10

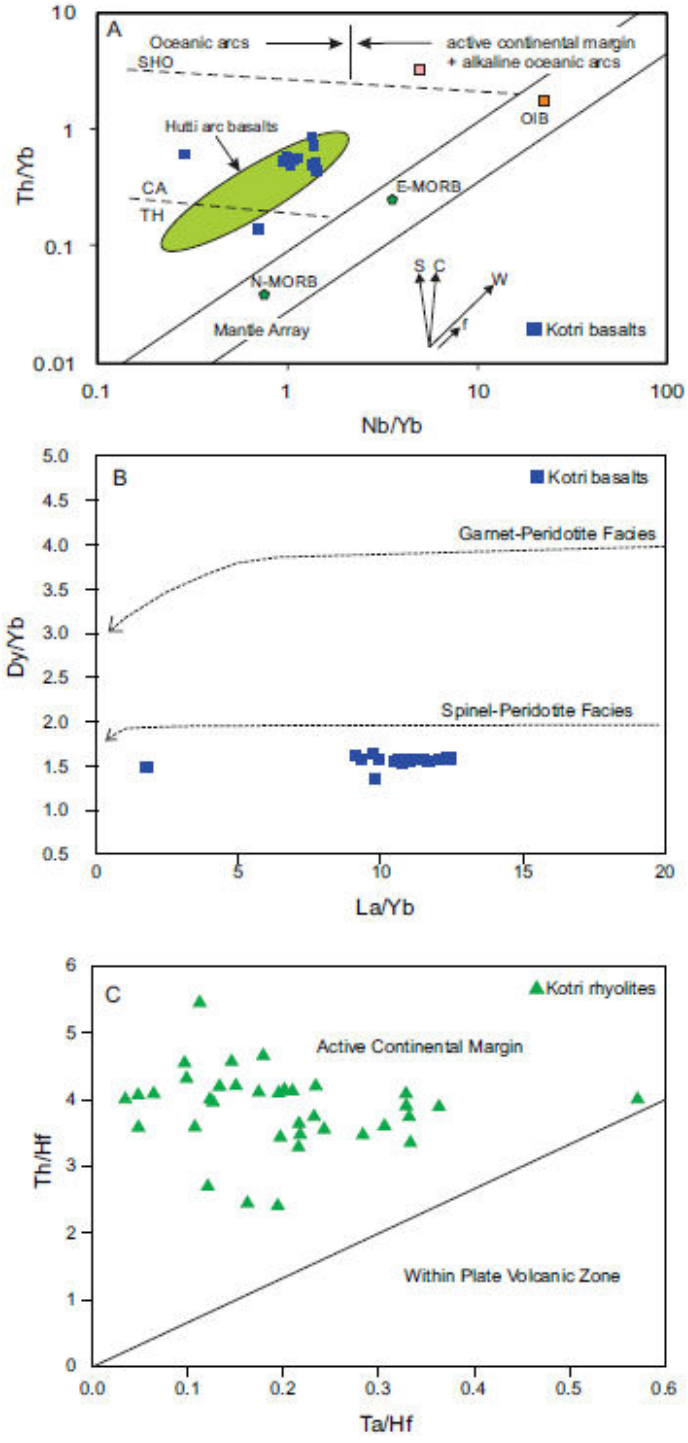

Fig. 11

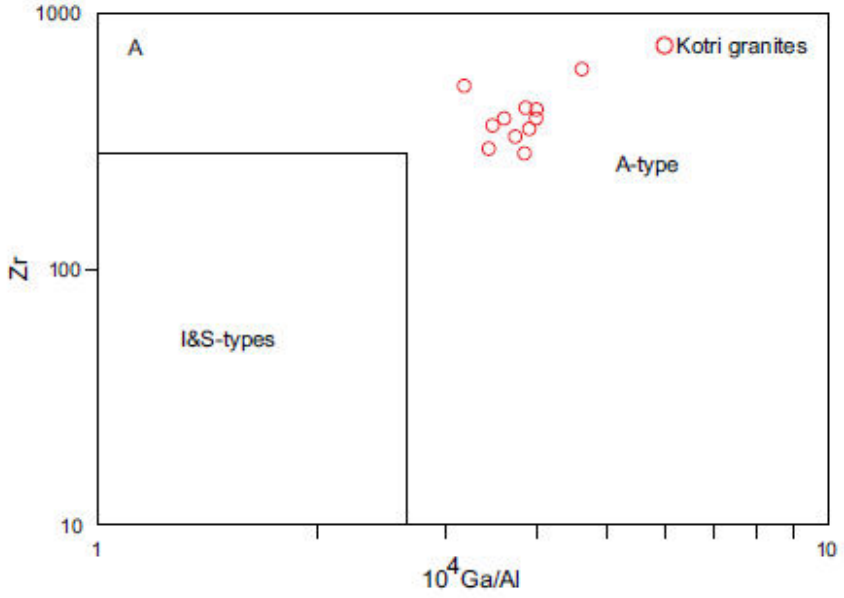

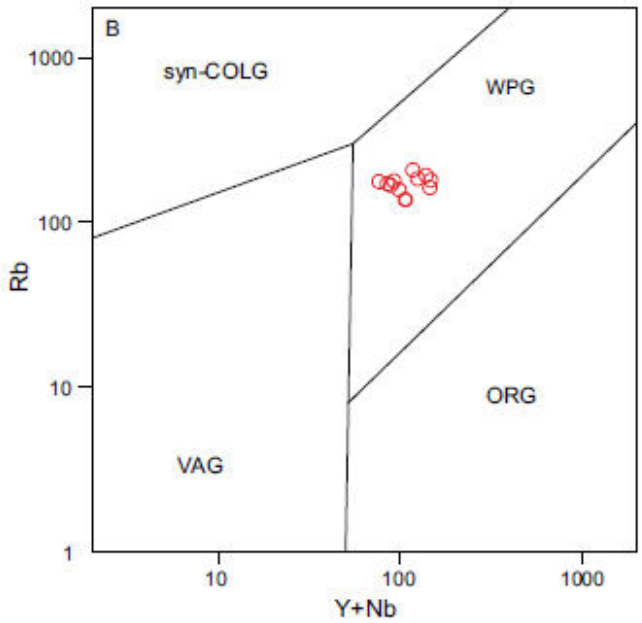

Fig. 12

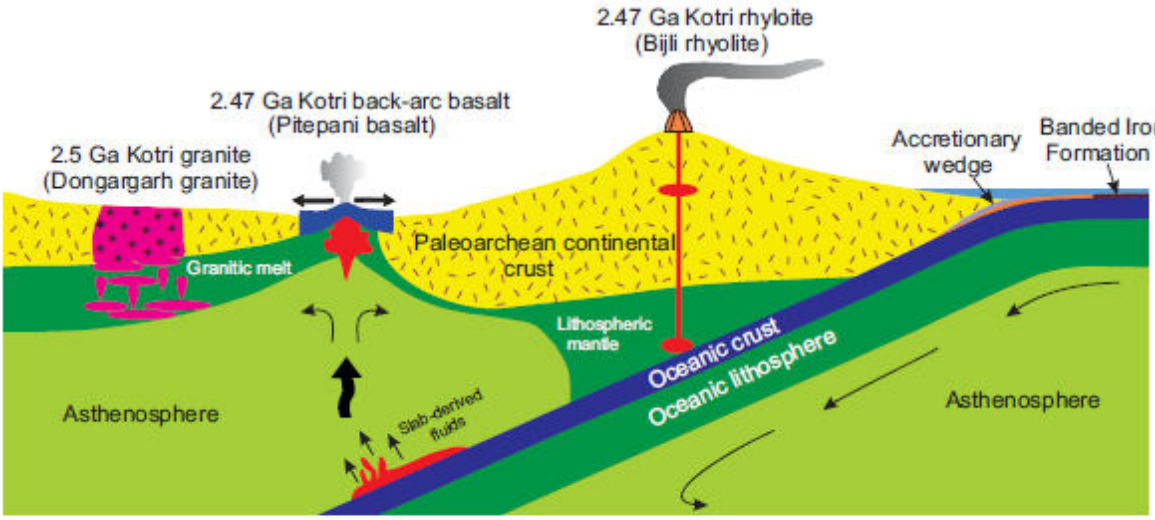

Fig. 13

Table 1. Major, trace and rare earth compositions of Kotri basalts

Table 1. (*Contd...*)

wt.%	KB 54	KB 55	KB 57	KB 59	KB 88	KB 91	KB 92	KB 95	KB 100(A)
SiO_2	51.02	49.77	51.51	50.70	50.04	50.75	49.93	48.19	50.74
TiO_2	0.73	1.08	0.91	1.05	1.29	1.24	1.14	1.08	1.34
Al_2O_3	14.50	12.52	12.23	13.12	11.84	12.16	12.74	12.31	11.70
Fe_2O_3	11.30	14.66	12.19	13.08	14.63	13.52	13.01	14.75	15.09
MnO	0.15	0.17	0.16	0.16	0.16	0.18	0.15	0.18	0.16
MgO	7.16	6.89	6.36	6.66	6.09	6.47	7.06	7.96	5.76
CaO	10.80	10.69	10.25	10.47	10.93	10.74	11.32	13.49	10.44
K_2O	2.77	2.97	2.73	2.93	2.72	2.73	2.22	1.63	3.08
Na_2O	1.37	0.27	1.63	1.02	1.31	1.17	1.11	0.23	1.32
P_2O_5	0.13	0.15	0.14	0.14	0.10	0.19	0.19	0.19	0.21
LOI	1.32	0.42	0.83	0.63	0.73	0.59	0.81	0.83	0.27
Sum	101.27	99.59	99.00	100.10	99.94	99.74	99.68	100.72	100.11
Mg#	41.09	34.10	36.48	35.99	31.43	34.50	37.40	37.27	29.59
ppm									

Table 1. (*Contd...*)

wt.%	KB 100(E)	KB 100(I)	KB 100(M)	KB 100(C1)	KB 100(C2)	KB 100(C4)	KB 100(C6)
SiO_2	47.37	49.73	50.26	50.22	51.76	50.15	50.60
TiO_2	1.77	1.71	1.47	1.29	1.30	1.34	1.33
Al_2O_3	12.49	12.43	11.71	11.71	11.60	11.80	11.83
Fe_2O_3	13.15	13.53	13.69	15.26	13.60	14.00	14.25
MnO	0.17	0.21	0.17	0.18	0.18	0.18	0.18
MgO	7.32	6.38	5.66	5.86	5.85	5.97	5.87
CaO	9.94	10.61	10.76	9.95	10.46	10.24	10.29
K_2O	2.86	2.26	3.62	2.97	2.81	2.90	2.82
Na_2O	3.74	2.13	1.47	1.53	1.71	1.66	1.65
P_2O_5	0.21	0.19	0.21	0.20	0.22	0.22	0.22
LOI	0.94	1.05	0.61	0.38	0.61	0.39	0.21
Sum	99.96	100.23	99.63	99.55	100.10	98.85	99.25
Mg#	38.00	34.17	31.28	29.71	32.14	31.95	31.20
ppm							

Table 1. (*Contd...*)

wt.%	KB 100(C8)	KB 100(C10)
SiO_2	54.03	51.35
TiO_2	0.35	1.37
Al_2O_3	13.27	12.00
Fe_2O_3	9.70	13.23
MnO	0.08	0.17
MgO	5.31	6.03
CaO	9.55	9.88
K_2O	1.84	3.06
Na_2O	4.22	1.87
P_2O_5	0.17	0.20
LOI	3.93	0.43
Sum	102.45	99.59
Mg#	37.60	33.41
ppm		

Cr	18.64	33.24	15.47	14.47	14.16	14.86	18.57	56.10	13.84	Cr	14.33	17.29	15.32	16.64	13.16	19.61	15.50	Cr	21.54	51.24
Co	36.04	52.89	44.59	44.78	51.93	52.32	50.16	57.74	54.82	Co	56.62	82.85	71.02	52.38	51.21	52.71	53.86	Co	39.09	29.89
Ni	12.35	24.72	13.99	13.10	17.80	18.42	24.94	32.44	17.84	Ni	22.10	17.65	16.91	16.09	17.03	16.43	17.94	Ni	13.53	46.20
Rb	37.87	1.38	42.27	22.13	39.60	32.26	31.19	3.63	64.16	Rb	55.07	181.42	85.61	39.46	52.97	52.43	53.50	Rb	37.63	74.62
Sr	337	338	311	370	408	377	350	120	386	Sr	300	333	267	298	312	331	346	Sr	350	172
Cs	2.07	0.12	0.50	0.88	5.69	6.71	1.33	0.43	11.75	Cs	8.13	47.94	19.34	6.24	10.54	10.31	9.61	Cs	2.24	4.30
Ba	255	181	490	284	486	409	300	43	669	Ba	932	1667	978	830	544	504	525	Ba	242	7622
Sc	28	38	30	27	33	33	31	46	37	Sc	42	52	45	38	38	40	42	Sc	33	26
V	150	173	157	128	202	189	153	256	239	V	300	373	313	236	234	264	282	V	167	164
Ta	0.28	0.34	0.21	0.35	0.18	0.29	0.24	0.15	0.29	Ta	0.22	0.02	0.36	0.27	0.34	0.30	0.30	Ta	0.20	0.26
Nb	6.37	10.30	8.84	10.65	6.88	8.08	7.55	3.54	8.31	Nb	7.06	1.51	10.81	7.36	8.42	8.66	8.16	Nb	6.03	7.67
Zr	113	156	165	167	207	166	186	77	170	Zr	233	250	240	167	163	170	164	Zr	107	174
Hf	2.63	3.47	3.56	3.82	4.81	3.88	4.80	2.12	4.00	Hf	5.27	5.52	5.14	3.74	3.84	3.98	3.89	Hf	2.44	4.17
Th	5.24	4.12	4.30	5.18	6.46	6.39	5.51	0.86	6.65	Th	6.89	9.55	8.91	6.29	6.47	6.75	6.71	Th	4.87	8.01
U	1.03	0.80	0.70	0.84	1.27	1.28	1.22	0.24	1.75	U	1.66	131.44	168.67	34.11	1.38	1.40	1.41	U	0.93	10.45
Y	17.15	27.38	25.60	28.79	31.84	31.10	31.55	24.72	30.98	Y	31.06	40.32	40.59	31.13	30.49	32.35	30.97	Y	16.47	22.20
La	21.15	23.86	22.26	26.66	33.75	32.51	30.18	4.42	33.84	La	35.00	48.19	42.57	32.86	32.98	34.06	33.13	La	19.69	24.76

Ce	40.70	46.22	44.49	52.23	66.85	65.03	62.24	11.11	67.64
Pr	3.67	4.39	4.23	5.03	6.44	6.21	6.03	1.32	6.38
Nd	17.00	21.31	20.58	24.97	31.64	30.54	29.64	8.19	30.52
Sm	3.95	5.19	4.94	5.96	7.29	7.04	6.87	2.59	6.99
Eu	0.98	1.40	1.28	1.49	1.72	1.72	1.49	0.91	1.64
Gd	3.19	4.61	4.26	5.09	5.76	5.55	5.50	3.38	5.43
Tb	0.50	0.75	0.70	0.83	0.91	0.89	0.89	0.63	0.88
Dy	2.68	4.19	3.76	4.46	4.96	4.79	4.73	3.71	4.75
Ho	0.56	0.87	0.79	0.94	1.02	0.99	1.01	0.80	0.99
Er	1.77	2.79	2.55	2.92	3.27	3.24	3.19	2.62	3.21
Tm	0.26	0.40	0.37	0.42	0.48	0.47	0.46	0.38	0.47
Yb	1.70	2.62	2.40	2.74	3.18	3.10	3.03	2.51	3.05
Lu	0.25	0.39	0.36	0.42	0.50	0.48	0.46	0.37	0.45
Cu	68	48	76	66	66	51	126	125	70
Pb	4.99	3.91	4.38	5.37	7.00	5.42	6.29	3.59	6.96
Zn	67	101	128	75	111	112	142	120	135
Ga	18	22	21	21	24	24	22	17	25

Table 1.

Ce	70.21	94.40	85.37	65.73	66.32	68.87	67.70
Pr	6.60	8.80	8.05	6.22	6.29	6.50	6.41
Nd	30.82	41.57	38.20	29.70	29.64	31.16	30.64
Sm	7.04	9.51	8.69	6.82	6.79	7.16	7.03
Eu	1.73	2.12	2.21	1.62	1.67	1.73	1.67
Gd	5.43	7.38	6.64	5.35	5.28	5.60	5.48
Tb	0.93	1.15	1.06	0.86	0.85	0.89	0.88
Dy	4.77	6.27	5.87	4.68	4.62	4.83	4.79
Ho	1.01	1.31	1.29	0.99	0.97	1.02	1.00
Er	3.23	4.27	4.37	3.20	3.16	3.29	3.25
Tm	0.47	0.62	0.65	0.47	0.46	0.48	0.47
Yb	3.04	3.99	4.34	3.05	2.99	3.11	3.06
Lu	0.44	0.58	0.62	0.45	0.44	0.47	0.45
Cu	90	220	98	69	68	94	67
Pb	6.41	7.41	7.64	6.09	5.81	5.07	6.02
Zn	153	173	179	108	113	100	119
Ga	26	34	30	25	25	26	25

Table 1.

Ce	37.33	45.55
Pr	3.43	4.02
Nd	15.86	18.43
Sm	3.69	4.46
Eu	0.93	1.25
Gd	2.98	3.91
Tb	0.47	0.60
Dy	2.55	3.28
Ho	0.53	0.69
Er	1.72	2.23
Tm	0.25	0.32
Yb	1.60	2.12
Lu	0.23	0.31
Cu	76	101
Pb	6.92	5.45
Zn	68	76
Ga	21	17

Table 1.

(*Contd...*)

	KB 54	KB 55	KB 57	KB 59	KB 88	KB 91	KB 92	KB 95	KB 100(A)
Na_2O+K_2O	4.16	3.24	4.42	3.95	4.03	3.90	3.33	1.84	4.40
Nb/Th	1.22	2.50	2.06	2.06	1.07	1.26	1.37	4.13	1.25
Zr/Hf	42.98	44.99	46.25	43.87	42.99	42.75	38.73	36.11	42.60
Zr/Y	6.58	5.70	6.43	5.82	6.50	5.33	5.89	3.10	5.50
Nb/Ta	22.43	30.29	42.31	30.69	37.82	28.23	32.12	23.91	28.28
Zr/Nb	17.72	15.14	18.62	15.73	30.04	20.52	24.60	21.63	20.51
Nb/Y	0.37	0.38	0.35	0.37	0.22	0.26	0.24	0.14	0.27
Nb/Th	1.22	2.50	2.06	2.06	1.07	1.26	1.37	4.13	1.25
Ba/Nb	39.98	17.60	55.45	26.62	70.60	50.65	39.70	12.07	80.43
Ba/La	12.04	7.60	22.03	10.63	14.40	12.58	9.93	9.65	19.76
La/Nb	3.32	2.22	2.52	2.50	4.90	4.03	4.00	1.25	4.07
Eu/Eu*	0.82	0.86	0.84	0.80	0.79	0.81	0.72	0.94	0.78
$(La/Yb)_N$	8.92	6.53	6.66	6.98	7.61	7.53	7.14	1.26	7.96
$(Tb/Yb)_N$	1.33	1.31	1.33	1.38	1.30	1.31	1.33	1.14	1.31
$(Gd/Yb)_N$	1.52	1.43	1.44	1.50	1.46	1.45	1.47	1.09	1.44

(*Contd...*)

	KB 100(E)	KB 100(I)	KB 100(M)	KB 100(C1)	KB 100(C2)	KB 100(C4)	KB 100(C6)
Na_2O+K_2O	6.60	4.39	5.09	4.50	4.52	4.56	4.47
Nb/Th	1.02	0.16	1.21	1.17	1.30	1.28	1.22
Zr/Hf	44.16	45.41	46.77	44.65	42.42	42.85	42.22
Zr/Y	7.49	6.21	5.92	5.36	5.35	5.27	5.30
Nb/Ta	32.08	100.67	29.95	27.14	24.69	28.86	27.12
Zr/Nb	32.98	165.85	22.21	22.69	19.37	19.69	20.12
Nb/Y	0.23	0.04	0.27	0.24	0.28	0.27	0.26
Nb/Th	1.02	0.16	1.21	1.17	1.30	1.28	1.22
Ba/Nb	132.08	1104.30	90.42	112.85	64.66	58.25	64.29
Ba/La	26.64	34.60	22.97	25.26	16.50	14.81	15.84
La/Nb	4.96	31.92	3.94	4.47	3.92	3.93	4.06
Eu/Eu*	0.82	0.75	0.85	0.79	0.82	0.81	0.79
$(La/Yb)_N$	8.26	8.66	7.03	7.72	7.90	7.87	7.77
$(Tb/Yb)_N$	1.39	1.31	1.11	1.28	1.29	1.30	1.30
$(Gd/Yb)_N$	1.45	1.50	1.24	1.42	1.43	1.46	1.45

(*Contd...*)

	KB 100(C8)	KB 100(C10)
Na_2O+K_2O	6.06	4.93
Nb/Th	1.24	0.96
Zr/Hf	43.90	41.64
Zr/Y	6.51	7.83
Nb/Ta	30.15	29.74
Zr/Nb	17.78	22.65
Nb/Y	0.37	0.35
Nb/Th	1.24	0.96
Ba/Nb	40.06	993.48
Ba/La	12.27	307.88
La/Nb	3.27	3.23
Eu/Eu*	0.83	0.90
$(La/Yb)_N$	8.81	8.36
$(Tb/Yb)_N$	1.34	1.29
$(Gd/Yb)_N$	1.50	1.49

$(La/Sm)_N$	3.34	2.87	2.82	2.79	2.89	2.89	2.74	1.07	3.02	$(La/Sm)_N$	3.10	3.16	3.06	3.01	3.03	2.97	2.94	$(La/Sm)_N$	3.33	3.47
Normalization factors after Sun and McDonough (1989)										Normalization factors after Sun and McDonough (1989)								Normalization factors after Sun and McDonough (1989)		

Table 2. Major , trace and rare earth element compositions of Kotri granites

wt.%	KB 126	KB 127	KB 128	KB 129	KB 184	KB 185	KB 186	KB 187	KB 188	KB 189	KB 190
SiO_2	73.59	73.06	73.74	71.22	73.13	72.52	72.33	69.10	72.86	74.08	72.61
TiO_2	0.18	0.16	0.18	0.35	0.16	0.13	0.28	0.18	0.29	0.20	0.15
Al_2O_3	10.77	11.34	10.80	11.47	11.29	11.72	11.33	12.62	10.87	10.61	11.59
Fe_2O_3	2.74	2.78	2.92	4.58	2.79	2.43	3.52	2.82	3.63	3.24	2.75
MnO	0.03	0.03	0.03	0.05	0.03	0.03	0.04	0.05	0.03	0.03	0.03
MgO	0.51	0.35	0.32	0.27	0.36	0.27	0.42	0.42	0.99	0.32	0.34
CaO	1.13	1.06	1.30	1.27	0.54	0.91	0.73	2.62	0.48	1.00	0.81
K_2O	6.72	7.36	6.76	6.60	7.25	7.32	6.25	7.38	6.66	7.11	7.33
Na_2O	3.04	3.22	3.11	3.60	3.36	3.42	3.04	3.70	3.14	2.79	3.26
P_2O_5	0.04	0.03	0.04	0.07	0.05	0.04	0.06	0.05	0.05	0.05	0.04
LOI	0.84	0.83	0.58	0.79	0.64	0.48	0.81	1.56	0.60	0.56	0.61
Sum	99.59	100.22	99.78	100.27	99.60	99.27	98.81	100.50	99.60	99.99	99.52
Mg#	3.74	3.78	3.92	5.58	3.79	3.43	4.52	3.82	4.63	4.24	3.75
ppm											
Cr	20.6	21.9	21.5	18.7	23.1	23.0	18.5	18.2	22.4	22.4	21.2
Co	2.6	2.7	2.7	3.1	3.0	2.7	3.1	2.7	3.1	3.5	2.6
Ni	1.6	1.6	1.6	1.6	1.7	1.7	1.5	1.6	1.6	1.6	1.6
Rb	137	184	162	176	171	178	158	207	192	180	168
Sr	51	51	75	99	60	83	74	109	73	71	74
Cs	2	2	4	14	2	2	2	2	3	4	1
Ba	910	873	990	1012	1148	1079	972	1165	1182	1185	1179
Sc	2.96	3.25	3.25	3.57	3.19	2.63	3.80	3.60	4.35	3.91	3.04
V	11.91	9.37	10.04	16.76	12.02	10.79	12.95	9.34	13.73	10.65	11.73
Ta	1.13	1.70	2.18	1.17	0.61	1.76	1.72	4.80	1.85	2.56	1.47
Nb	30.13	36.86	47.15	27.15	23.28	27.71	37.32	38.87	47.20	40.57	30.35
Zr	366	284	355	522	389	331	429	423	608	389	297
Hf	11	10	11	13	12	11	13	13	17	12	9
Th	28	30	32	27	29	29	31	32	41	31	20
U	6	8	8	6	6	7	5	5	6	7	4
Y	77	88	99	49	62	65	61	79	92	107	58
La	115.05	119.30	144.05	78.39	123.25	143.47	116.04	182.50	191.57	190.95	100.01
Ce	218.77	233.06	273.72	142.06	231.24	234.32	267.67	299.04	342.13	273.33	178.80
Pr	21.98	23.05	26.72	13.71	22.02	24.63	21.96	31.62	33.18	32.27	18.03
Nd	80.96	85.82	98.29	48.97	79.04	86.81	79.24	113.71	118.80	119.84	65.75
Sm	15.16	16.67	18.36	8.33	13.14	13.62	13.84	21.38	19.78	21.32	11.70
Eu	1.70	1.66	1.97	1.89	1.97	1.97	1.82	2.14	2.55	2.79	1.92
Gd	11.31	12.56	13.89	6.18	9.23	9.43	9.58	13.40	13.81	16.21	8.59
Tb	2.00	2.24	2.46	1.08	1.56	1.56	1.67	2.18	2.31	2.75	1.47
Dy	13.69	15.53	17.25	7.62	10.68	10.67	11.42	14.16	15.81	18.86	10.10
Ho	2.58	2.93	3.26	1.57	2.10	2.19	2.27	2.65	3.10	3.63	1.99
Er	6.49	7.40	8.25	4.21	5.46	5.85	5.92	6.63	8.03	9.31	5.16

Tm	0.92	1.05	1.17	0.62	0.79	0.85	0.86	0.94	1.15	1.33	0.74
Yb	5.82	6.65	7.41	4.05	5.08	5.61	5.54	5.90	7.44	8.50	4.80
Lu	0.92	1.05	1.17	0.67	0.83	0.94	0.89	0.99	1.21	1.35	0.77
Cu	0.53	0.58	0.59	0.64	0.63	0.59	0.54	0.59	0.61	0.59	0.55
Pb	34.25	51.34	51.05	46.02	54.51	56.05	44.42	47.08	35.27	54.70	47.57
Zn	22.01	26.17	29.68	36.69	30.98	33.23	30.70	30.14	37.04	36.72	29.84
Ga	19.83	23.08	22.32	19.31	21.55	23.17	23.15	26.67	26.51	22.40	21.08

Table 2. (*Contd...*)

	KB 126	KB 127	KB 128	KB 129	KB 184	KB 185	KB 186	KB 187	KB 188	KB 189	KB 190
Na_2O+K_2O	9.76	10.58	9.87	10.20	10.61	10.74	9.29	11.08	9.80	9.90	10.59
Fe*	1.74	1.82	1.93	3.10	1.82	1.60	2.31	1.82	2.21	2.15	1.80
A/NK	1.10	1.07	1.09	1.12	1.06	1.09	1.22	1.14	1.11	1.07	1.09
A/CNK	0.99	0.97	0.97	1.00	1.01	1.01	1.13	0.92	1.06	0.97	1.02
$(La/Yb)_N$	14.19	12.87	13.93	13.89	17.41	18.35	15.01	22.18	18.46	16.10	14.94
$(Gd/Yb)_N$	1.57	1.53	1.52	1.23	1.47	1.36	1.40	1.84	1.50	1.54	1.45
Eu/Eu*	0.38	0.34	0.36	0.77	0.52	0.50	0.46	0.36	0.45	0.44	0.56

Normalization factors after Sun and McDonough (1989)

Table 3. Zircon U-Pb analytical data of sample Kotri basalt

Sample	Element concentration(ppm)				Isotope ratios (±1σ)						Age (Ma±1σ)						Concordance
Spots	Pb	Th	U	Th/U	$^{207}Pb/^{206}Pb$		$^{207}Pb/^{235}U$		$^{206}Pb/^{238}U$		$^{207}Pb/^{206}Pb$		$^{207}Pb/^{235}U$		$^{206}Pb/^{238}U$		(%)
KB-55 (Basalt)																	
KB-55-1	57	38	107	0.36	0.161	0.002	10.5961	0.146	0.4774	0.0047	2466	21	2488	34	2516	25	98
KB-55-2	153	137	278	0.49	0.1618	0.0019	10.7547	0.1436	0.482	0.0047	2475	20	2502	33	2536	25	98
KB-55-3	58	39	109	0.36	0.1664	0.002	10.9805	0.1522	0.4786	0.0047	2522	20	2521	35	2521	25	100
KB-55-4	113	106	213	0.5	0.1616	0.0019	10.5184	0.1408	0.4722	0.0047	2472	20	2482	33	2493	25	99
KB-55-5	111	95	210	0.45	0.1615	0.0019	10.5367	0.1394	0.4732	0.0046	2471	20	2483	33	2498	24	99
KB-55-6	73	58	138	0.42	0.1609	0.0019	10.6789	0.1417	0.4815	0.0047	2465	20	2496	33	2534	25	97
KB-55-7	155	132	285	0.46	0.1607	0.0019	10.8429	0.1436	0.4895	0.0047	2463	20	2510	33	2568	25	96
KB-55-8	75	58	141	0.41	0.1623	0.0019	10.6815	0.1438	0.4772	0.0046	2480	20	2496	34	2515	24	99
KB-55-9	221	210	402	0.52	0.1604	0.0019	10.865	0.1452	0.4913	0.0048	2460	20	2512	34	2576	25	95
KB-55-10	88	75	164	0.46	0.1603	0.0019	10.7549	0.1436	0.4865	0.0047	2459	20	2502	33	2556	25	96
KB-55-11	172	157	317	0.5	0.1613	0.0019	10.8213	0.1428	0.4867	0.0047	2469	20	2508	33	2556	25	97
KB-55-12	89	82	168	0.49	0.1614	0.0019	10.6282	0.141	0.4775	0.0046	2471	20	2491	33	2516	24	98
KB-55-13	86	69	159	0.44	0.1605	0.0019	10.9003	0.1444	0.4927	0.0048	2461	20	2515	33	2582	25	95
KB-55-14	79	71	147	0.48	0.1601	0.0019	10.6985	0.1434	0.4847	0.0047	2457	20	2497	33	2548	25	96
KB-55-15	78	83	144	0.58	0.1591	0.0019	10.5447	0.1427	0.4807	0.0047	2446	20	2484	34	2530	25	97
KB-55-16	80	82	148	0.55	0.1598	0.0019	10.6474	0.1454	0.4832	0.0047	2454	21	2493	34	2541	25	97
KB-55-17	109	66	209	0.32	0.165	0.002	10.9953	0.1502	0.4832	0.0047	2508	20	2523	34	2541	25	99
KB-55-18	50	46	94	0.49	0.1614	0.002	10.6306	0.1454	0.4777	0.0047	2470	21	2491	34	2517	25	98
KB-55-19	100	113	189	0.6	0.1601	0.0019	10.3077	0.1383	0.4669	0.0045	2457	20	2463	33	2470	24	99
KB-55-20	87	11	177	0.06	0.1609	0.0019	10.6539	0.1426	0.4802	0.0047	2465	20	2493	33	2528	25	98
KB-55-21	99	120	183	0.66	0.1608	0.0019	10.5303	0.1404	0.4748	0.0046	2465	20	2483	33	2505	24	98
KB-55-22	97	104	180	0.58	0.1612	0.0019	10.604	0.1421	0.4772	0.0046	2468	20	2489	33	2515	24	98
KB-55-23	75	76	141	0.54	0.1597	0.0019	10.5043	0.1427	0.477	0.0046	2453	21	2480	34	2514	24	98
KB-55-24	111	127	203	0.62	0.1611	0.002	10.6295	0.1461	0.4785	0.0047	2467	21	2491	34	2521	25	98
KB-55-25	81	80	153	0.52	0.1604	0.002	10.3824	0.1431	0.4695	0.0046	2460	21	2469	34	2481	24	99

KB-55-26	104	108	192	0.56	0.1626	0.002	10.68	0.145	0.4765	0.0046	2483	20	2496	34	2512	24	99
KB-55-28	117	110	213	0.52	0.1627	0.0019	10.8698	0.1445	0.4846	0.0047	2484	20	2512	33	2547	25	97
KB-55-29	108	113	195	0.58	0.1623	0.0019	10.7295	0.1437	0.4796	0.0047	2479	20	2500	33	2525	25	98
KB-55-30	107	107	190	0.56	0.1619	0.0019	10.8897	0.1449	0.4878	0.0047	2476	20	2514	33	2561	25	97
KB-55-31	118	123	209	0.59	0.1639	0.0019	10.9747	0.1469	0.4857	0.0047	2496	20	2521	34	2552	25	98
KB-55-32	159	168	279	0.6	0.1615	0.0019	10.8114	0.1469	0.4856	0.0048	2471	20	2507	34	2552	25	97

Table 3. (*Contd...*) Zircon U-Pb analytical data of sample Kotri rhyolites

Sample	Element concentration(ppm)				Isotope ratios (±1σ)						Age (Ma±1σ)						Concordance
Spots	Pb	Th	U	Th/U	$^{207}Pb/^{206}Pb$		$^{207}Pb/^{235}U$		$^{206}Pb/^{238}U$		$^{207}Pb/^{206}Pb$		$^{207}Pb/^{235}U$		$^{206}Pb/^{238}U$		(%)
KB-26 (Rhyolite)																	
KB-26-1	253	220	494	0.45	0.1634	0.002	10.4538	0.1423	0.4639	0.0045	2492	20	2476	34	2457	24	99
KB-26-2	245	244	482	0.51	0.1629	0.0019	10.2388	0.1391	0.4557	0.0045	2486	20	2457	33	2421	24	97
KB-26-3	195	233	357	0.65	0.1633	0.0019	10.7885	0.144	0.4791	0.0046	2490	20	2505	33	2523	24	99
KB-26-4	205	284	404	0.7	0.1591	0.0019	9.7202	0.1309	0.4432	0.0043	2446	20	2409	32	2365	23	97
KB-26-5	134	166	248	0.67	0.1632	0.0019	10.6741	0.1432	0.4743	0.0046	2489	20	2495	33	2503	24	99
KB-26-6	86	87	163	0.53	0.1636	0.002	10.737	0.145	0.4761	0.0046	2493	20	2501	34	2510	24	99
KB-26-7	90	90	168	0.53	0.1624	0.002	10.8402	0.1473	0.4843	0.0047	2480	20	2510	34	2546	25	97
KB-26-8	74	71	137	0.52	0.162	0.002	10.9274	0.1506	0.4892	0.0048	2477	21	2517	35	2567	25	96
KB-26-9	72	63	133	0.48	0.1626	0.002	11.1222	0.1545	0.4962	0.0048	2482	21	2533	35	2598	25	96
KB-26-10	142	138	248	0.56	0.1619	0.002	11.3842	0.1548	0.5099	0.0049	2476	21	2555	35	2656	26	93
KB-26-11	183	168	330	0.51	0.161	0.0019	11.1132	0.1499	0.5006	0.0048	2466	20	2533	34	2616	25	94
KB-26-12	74	75	139	0.54	0.1627	0.002	10.8681	0.1488	0.4846	0.0048	2484	20	2512	34	2547	25	98
KB-26-13	159	151	290	0.52	0.1607	0.0019	11.0291	0.1498	0.4978	0.0048	2463	20	2526	34	2605	25	95
KB-26-14	142	145	254	0.57	0.1609	0.002	11.1447	0.1537	0.5024	0.0049	2465	21	2535	35	2624	25	94
KB-26-15	186	176	340	0.52	0.1596	0.002	10.8266	0.1518	0.492	0.0048	2451	21	2508	35	2579	25	95
KB-26-18	198	208	448	0.46	0.1557	0.002	8.6417	0.1216	0.4027	0.0039	2409	21	2301	32	2181	21	90
KB-26-19	122	86	220	0.39	0.1608	0.002	11.0655	0.1536	0.4991	0.0049	2464	21	2529	35	2610	25	94
KB-26-20	57	7	111	0.06	0.1625	0.002	11.2582	0.156	0.5025	0.0049	2482	21	2545	35	2625	26	95
KB-26-21	87	74	155	0.48	0.1639	0.002	11.3426	0.1547	0.5018	0.0049	2497	20	2552	35	2622	26	95

KB-26-22	194	192	345	0.56	0.1637	0.002	11.2384	0.1533	0.498	0.0048	2494	20	2543	35	2605	25	96
KB-26-23	132	127	244	0.52	0.1631	0.002	10.774	0.1478	0.479	0.0046	2488	21	2504	34	2523	24	99
KB-26-25	132	109	243	0.45	0.1653	0.0021	11.1011	0.1557	0.487	0.0048	2511	21	2532	35	2558	25	98
KB-26-26	108	85	197	0.43	0.1661	0.002	11.2031	0.1543	0.4893	0.0048	2518	21	2540	35	2568	25	98
KB-26-27	74	62	141	0.44	0.1681	0.0022	10.8185	0.1566	0.4669	0.0045	2538	22	2508	36	2470	24	97
KB-26-28	167	191	290	0.66	0.1656	0.002	11.2356	0.1517	0.492	0.0048	2514	20	2543	34	2579	25	97
KB-26-29	126	103	229	0.45	0.1657	0.002	11.2265	0.1516	0.4914	0.0048	2515	20	2542	34	2577	25	98
KB-26-30	196	181	360	0.5	0.1645	0.002	11.0059	0.1487	0.4852	0.0047	2503	20	2524	34	2550	25	98
KB-26-31	231	203	428	0.47	0.165	0.002	10.9889	0.1506	0.4831	0.0047	2507	20	2522	35	2541	25	99
KB-26-32	181	186	333	0.56	0.1646	0.002	10.8623	0.1507	0.4786	0.0047	2504	21	2511	35	2521	25	99

Table 3. (*Contd...*) Zircon U-Pb analytical data of sample Kotri rhyolites

Sample	Element concentration(ppm)				Isotope ratios (±1σ)						Age (Ma±1σ)						Concordance
Spots	Pb	Th	U	Th/U	$^{207}Pb/^{206}Pb$		$^{207}Pb/^{235}U$		$^{206}Pb/^{238}U$		$^{207}Pb/^{206}Pb$		$^{207}Pb/^{235}U$		$^{206}Pb/^{238}U$		(%)
KB-35(Rhyolite)																	
KB-35-1	209	162	393	0.41	0.1626	0.002	10.9195	0.1521	0.487	0.0048	2483	21	2516	35	2558	25	97
KB-35-2	140	106	259	0.41	0.1632	0.002	11.1553	0.1538	0.4957	0.0049	2489	20	2536	35	2595	25	96
KB-35-3	163	133	309	0.43	0.163	0.002	10.8615	0.1475	0.4834	0.0047	2487	20	2511	34	2542	25	98
KB-35-4	170	158	329	0.48	0.1624	0.0019	10.5513	0.1425	0.4711	0.0046	2481	20	2484	34	2488	24	100
KB-35-5	200	174	386	0.45	0.162	0.0019	10.6146	0.1431	0.4752	0.0046	2477	20	2490	34	2506	24	99
KB-35-6	227	201	430	0.47	0.1622	0.0019	10.7948	0.1478	0.4827	0.0048	2478	20	2506	34	2539	25	98
KB-35-7	252	259	461	0.56	0.1636	0.002	11.0422	0.1519	0.4894	0.0048	2494	20	2527	35	2568	25	97
KB-35-8	302	418	572	0.73	0.1651	0.002	10.725	0.1506	0.4711	0.0046	2509	21	2500	35	2488	25	99
KB-35-9	219	230	422	0.54	0.161	0.002	10.429	0.1448	0.4699	0.0046	2466	21	2474	34	2483	24	99
KB-35-10	196	184	373	0.49	0.1616	0.002	10.631	0.1453	0.4771	0.0046	2473	20	2491	34	2514	24	98
KB-35-11	214	256	411	0.62	0.1602	0.0019	10.2151	0.141	0.4626	0.0046	2457	20	2454	34	2451	25	100
KB-35-12	181	184	333	0.55	0.1611	0.0019	10.7621	0.1446	0.4845	0.0047	2467	20	2503	34	2547	25	97
KB-35-13	153	143	284	0.5	0.1607	0.0019	10.7182	0.1439	0.4837	0.0047	2463	20	2499	34	2543	25	97
KB-35-14	160	135	293	0.46	0.1609	0.0019	10.9316	0.1483	0.4927	0.0048	2465	20	2517	34	2582	25	95
KB-35-15	178	141	323	0.44	0.1607	0.0019	10.9477	0.1484	0.4941	0.0047	2463	20	2519	34	2588	25	95

KB-35-16	125	137	216	0.63	0.1606	0.002	10.8722	0.1513	0.4909	0.0048	2462	21	2512	35	2575	25	96
KB-35-17	196	115	363	0.32	0.1605	0.002	10.9308	0.1501	0.4939	0.0047	2461	21	2517	35	2587	25	95
KB-35-18	132	111	231	0.48	0.1607	0.002	11.1006	0.1512	0.501	0.0048	2463	21	2532	34	2618	25	94
KB-35-19	121	112	218	0.51	0.1618	0.0019	10.7897	0.1459	0.4836	0.0047	2475	20	2505	34	2543	25	97
KB-35-20	174	22	349	0.06	0.1608	0.0019	10.8315	0.1452	0.4884	0.0047	2464	20	2509	34	2564	25	96
KB-35-21	123	101	226	0.45	0.1611	0.0019	10.8012	0.1448	0.4862	0.0047	2468	20	2506	34	2554	25	97
KB-35-22	160	138	292	0.47	0.1616	0.0019	10.8328	0.1466	0.4861	0.0047	2473	20	2509	34	2554	25	97
KB-35-23	263	255	472	0.54	0.1611	0.0019	10.8686	0.1479	0.4892	0.0047	2468	20	2512	34	2567	25	96
KB-35-24	182	121	322	0.37	0.1624	0.002	11.377	0.1563	0.5082	0.0049	2480	21	2555	35	2649	25	94
KB-35-25	137	86	275	0.31	0.1606	0.002	9.9527	0.1372	0.4494	0.0043	2462	21	2430	34	2393	23	97
KB-35-26	141	95	243	0.39	0.1636	0.002	11.5584	0.1569	0.5124	0.0049	2493	20	2569	35	2667	26	93
KB-35-27	150	132	240	0.55	0.1638	0.002	11.9082	0.1616	0.5273	0.0051	2495	20	2597	35	2730	26	91
KB-35-28	194	119	319	0.37	0.1645	0.002	12.0017	0.1608	0.529	0.0051	2503	20	2605	35	2737	26	91
KB-35-29	216	180	346	0.52	0.1645	0.002	11.742	0.1586	0.5177	0.005	2502	20	2584	35	2690	26	93
KB-35-30	119	62	200	0.31	0.1657	0.002	11.9242	0.1627	0.5218	0.005	2515	21	2598	35	2707	26	93
KB-35-31	211	98	352	0.28	0.1649	0.002	12.1632	0.1672	0.5348	0.0051	2507	21	2617	36	2762	27	91
KB-35-32	134	61	225	0.27	0.1666	0.0021	12.0819	0.1696	0.5261	0.0051	2523	21	2611	37	2725	26	93

Table 3. (*Contd...*) Zircon U-Pb analytical data of sample Kotri granite

Sample	Element concentration(ppm)				Isotope ratios (±1σ)						Age (Ma±1σ)						Concordance
Spots	Pb	Th	U	Th/U	$^{207}Pb/^{206}Pb$		$^{207}Pb/^{235}U$		$^{206}Pb/^{238}U$		$^{207}Pb/^{206}Pb$		$^{207}Pb/^{235}U$		$^{206}Pb/^{238}U$		(%)
KB-127A(Granite)																	
KB-127A-1	278	637	1471	0.43	0.1159	0.0015	2.6353	0.0398	0.165	0.0017	1893	23	1311	20	984	10	67
KB-127A-3	351	272	696	0.39	0.187	0.0022	10.7397	0.1515	0.4166	0.0043	2716	20	2501	35	2245	23	79
KB-127A-4	45	44	77	0.56	0.1706	0.0021	11.4306	0.1608	0.4859	0.0049	2564	21	2559	36	2553	26	100
KB-127A-7	78	79	128	0.62	0.1829	0.0022	12.1523	0.1673	0.4818	0.005	2680	20	2616	36	2535	26	94
KB-127A-8	146	143	246	0.58	0.1809	0.0022	11.8808	0.1662	0.4764	0.0049	2661	20	2595	36	2511	26	94
KB-127A-9	198	149	346	0.43	0.1733	0.0021	11.5529	0.1595	0.4835	0.0049	2590	20	2569	35	2542	26	98
KB-127A-11	235	206	390	0.53	0.1858	0.0022	12.0629	0.1625	0.471	0.0049	2705	20	2609	35	2488	26	91
KB-127A-12	116	89	205	0.43	0.164	0.0019	11.1985	0.1495	0.4952	0.005	2497	20	2540	34	2593	26	96

KB-127A-13	113	80	192	0.42	0.1696	0.002	11.6919	0.1561	0.5001	0.005	2553	20	2580	34	2614	26	98
KB-127A-14	109	79	169	0.46	0.2027	0.0025	13.5541	0.1852	0.4849	0.0048	2848	20	2719	37	2549	25	88
KB-127A-15	231	204	635	0.32	0.1562	0.0019	6.7773	0.0922	0.3147	0.0032	2415	20	2083	28	1764	18	63
KB-127A-16	129	92	235	0.39	0.1637	0.002	10.4598	0.1468	0.4635	0.0049	2494	21	2476	35	2455	26	98
KB-127A-17	74	40	127	0.32	0.1733	0.0021	12.0114	0.1653	0.5026	0.005	2590	21	2605	36	2625	26	99
KB-127A-18	205	298	540	0.55	0.1665	0.002	6.9275	0.0936	0.3017	0.003	2523	20	2102	28	1700	17	52
KB-127A-19	178	137	363	0.38	0.1598	0.0019	9.5455	0.1315	0.4332	0.0046	2454	20	2392	33	2320	24	94
KB-127A-20	216	46	740	0.06	0.1555	0.0019	6.0919	0.0879	0.2842	0.0036	2407	20	1989	29	1612	20	51
KB-127A-21	117	122	223	0.55	0.1601	0.0019	9.9559	0.1334	0.4511	0.0045	2456	20	2431	33	2400	24	98
KB-127A-25	138	135	287	0.47	0.1556	0.0019	9.2462	0.1313	0.431	0.0045	2408	21	2363	34	2310	24	96
KB-127A-26	79	75	143	0.53	0.1606	0.0019	10.773	0.1463	0.4864	0.0049	2462	20	2504	34	2555	26	96
KB-127A-27	156	143	296	0.48	0.1603	0.0019	10.4847	0.1408	0.4744	0.0048	2459	20	2479	33	2503	25	98
KB-127A-28	162	138	295	0.47	0.1677	0.002	11.1492	0.1497	0.4822	0.0049	2535	20	2536	34	2537	26	100
KB-127A-29	103	108	187	0.58	0.1618	0.0019	10.8694	0.1464	0.4873	0.005	2474	20	2512	34	2559	26	97
KB-127A-30	104	89	189	0.47	0.1807	0.0022	11.6984	0.1595	0.4696	0.0047	2659	20	2581	35	2482	25	93
KB-127A-31	146	104	232	0.45	0.2251	0.0027	14.881	0.2054	0.4795	0.0049	3017	20	2808	39	2525	26	81
KB-127A-32	61	57	96	0.6	0.2026	0.0026	14.0236	0.1979	0.502	0.0051	2847	21	2751	39	2622	26	91

Table 4. Lu-Hf data of Zircon grains of Kotri basalt, rhyolites and granite

Sample Spots	Age (Ma)	$^{176}Yb/^{177}Hf$	$^{176}Lu/^{177}Hf$	$^{176}Hf/^{177}Hf$	2s	$^{176}Hf/^{177}Hf_i$	$e_{Hf}(0)$	$e_{Hf}(t)$	T_{DM} (Ma)	T_{DM}^{C} (Ma)	$f_{Lu/Hf}$
KB-55 (Basalt)											
KB-55-04	2471	0.0286	0.001	0.280972	0.000029	0.280925	-63.6	-10	3171	3589	-0.97
KB-55-05	2471	0.0133	0.0005	0.280992	0.000021	0.28097	-62.9	-8.4	3100	3491	-0.99
KB-55-09	2471	0.0362	0.0012	0.281001	0.000022	0.280944	-62.6	-9.3	3149	3548	-0.96
KB-55-19	2471	0.018	0.0006	0.281033	0.000023	0.281004	-61.5	-7.2	3057	3418	-0.98
KB-55-21	2471	0.0175	0.0006	0.281005	0.000024	0.280977	-62.5	-8.2	3093	3476	-0.98
KB-55-26	2471	0.0177	0.0006	0.281034	0.000023	0.281005	-61.5	-7.2	3056	3416	-0.98
KB-55-30	2471	0.0166	0.0006	0.281046	0.000021	0.281018	-61	-6.7	3038	3387	-0.98
KB-55-31	2471	0.0203	0.0007	0.281009	0.000021	0.280976	-62.4	-8.2	3097	3479	-0.98
KB-26 (Rhyolite)											
KB-26-01	2479	0.0216	0.0008	0.281013	0.00002	0.280978	-62.2	-7.9	3094	3469	-0.98
KB-26-07	2479	0.0256	0.0009	0.280991	0.000022	0.280949	-63	-9	3135	3531	-0.97
KB-26-11	2479	0.0262	0.0009	0.281028	0.00002	0.280987	-61.7	-7.6	3083	3449	-0.97
KB-26-12	2479	0.0434	0.0014	0.281022	0.000022	0.280955	-61.9	-8.8	3137	3519	-0.96
KB-26-15	2479	0.023	0.0008	0.281038	0.000019	0.281001	-61.3	-7.1	3063	3418	-0.98
KB-26-22	2479	0.0262	0.0008	0.28102	0.00002	0.28098	-62	-7.8	3092	3463	-0.97
KB-26-26	2479	0.0307	0.001	0.28105	0.000023	0.281004	-60.9	-7	3062	3412	-0.97

KB-26-30	2479	0.0226	0.0007	0.28099	0.00002	0.280956	-63	-8.7	3124	3517	-0.98
KB-26-31	2479	0.0242	0.0008	0.281057	0.000019	0.28102	-60.7	-6.4	3038	3377	-0.98
KB-26-32	2479	0.0389	0.0012	0.280977	0.000024	0.280919	-63.5	-10	3182	3596	-0.96
KB-35(Rhyolite)											
KB-35-05	2463	0.0346	0.0012	0.281054	0.000028	0.281	-60.7	-7.5	3072	3432	-0.96
KB-35-07	2463	0.0196	0.0007	0.281135	0.000022	0.281103	-57.9	-3.9	2925	3208	-0.98
KB-35-08	2463	0.0541	0.0019	0.281177	0.000027	0.28109	-56.4	-4.3	2958	3236	-0.94
KB-35-09	2463	0.0215	0.0007	0.281102	0.000019	0.281068	-59.1	-5.1	2973	3285	-0.98
KB-35-10	2463	0.0259	0.0009	0.281135	0.000023	0.281093	-57.9	-4.2	2942	3230	-0.97
KB-35-15	2463	0.0197	0.0007	0.281074	0.000021	0.281042	-60.1	-6	3008	3341	-0.98
KB-35-17	2463	0.0273	0.0009	0.281119	0.000022	0.281076	-58.4	-4.8	2965	3267	-0.97
KB-35-23	2463	0.0203	0.0007	0.281073	0.000021	0.281041	-60.1	-6.1	3009	3344	-0.98
KB-35-25	2463	0.0246	0.0008	0.281104	0.000022	0.281067	-59	-5.1	2975	3286	-0.98
KB-35-26	2463	0.021	0.0007	0.281126	0.000021	0.281092	-58.2	-4.2	2940	3231	-0.98
KB-127A(Granite)											
KB-127A-03	2506	0.0281	0.0009	0.281007	0.000024	0.280964	-62.4	-7.8	3115	3482	-0.97
KB-127A-11	2506	0.0325	0.001	0.281004	0.000018	0.280955	-62.5	-8.1	3130	3502	-0.97
KB-127A-14	2506	0.0204	0.0007	0.281095	0.000025	0.281062	-59.3	-4.3	2979	3269	-0.98
KB-127A-16	2506	0.0313	0.001	0.281091	0.000021	0.281044	-59.4	-5	3008	3309	-

KB-127A-17	2506	0.022	0.0007	0.281039	0.00002	0.281004	-61.3	-6.4	3058	3395	0.97 - 0.98
KB-127A-22	2506	0.0724	0.0019	0.281029	0.000021	0.280937	-61.6	-8.8	3170	3541	- 0.94
KB-127A-25	2506	0.0324	0.001	0.281038	0.000021	0.280991	-61.3	-6.9	3080	3424	- 0.97
KB-127A-26	2506	0.0351	0.001	0.281104	0.00002	0.281054	-59	-4.6	2995	3287	- 0.97
KB-127A-27	2506	0.0176	0.0006	0.281071	0.000018	0.281044	-60.2	-5	3002	3309	- 0.98
KB-127A-30	2506	0.0176	0.0006	0.281025	0.000021	0.280999	-61.8	-6.6	3063	3407	- 0.98

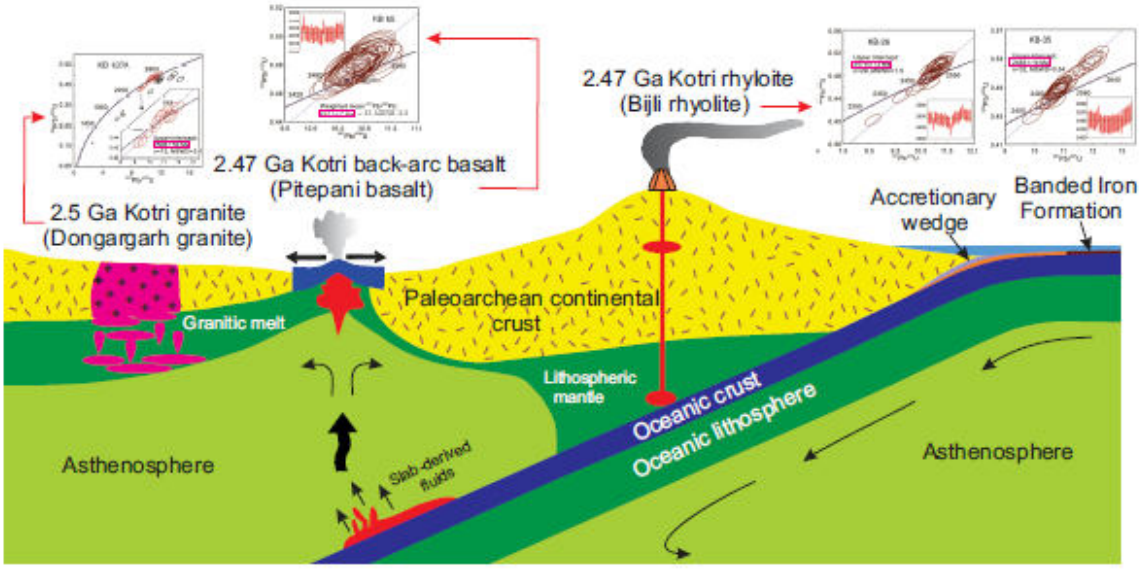

Graphical Abstract

Research Highlights:

- First report of U-Pb zircon age of mafic rocks (2.47 Ga) from the Kotri-Dongargarh Supergroup
- U-Pb age of Bijli rhyolite (2.46-2.48 Ga) and Dongargarh granite (2.5 Ga) exposed in Kotri belt
- Role of Paleo-Mesoarchean subducted crust in the crustal growth of Central Indian Bastar Craton
- Bimodal volcanism and granitoid emplacement in continental arc-back arc setting